Optical Properties of Graphene – Effect of Compressive Strain

A project report submitted

as a part of requirements for the degree of

MASTER OF SCIENCE

By

MANODEEP MONDAL

Roll no. PH13M1007

Under the supervision of

Dr. J.Suryanarayana

भारतीय प्रौद्योगिकी संस्थान हैदराबाद
Indian Institute of Technology Hyderabad

DEPARTMENT OF PHYSICS

INDIAN INSTITUTE OF TECHNOLOGY HYDERABAD

INDIA

APRIL 2015

Declaration

I hereby declare that the matter embodied in this report is the result of investigation carried out by me in the Department of Physics, Indian Institute of Technology Hyderabad under the supervision of **Dr. J. Suryanarayana**.

In keeping with general practice of reporting scientific observations, due acknowledgement has been made wherever the work described is based on the findings of other investigators.

Manodeep Mondal.

(Signature)

Manodeep Mondal

Roll No. : PH13M1007
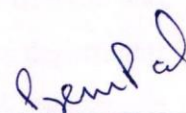
(Signature of supervisor)

Dr. J. Suryanarayana

Assistant Professor

Department of Physics

IIT Hyderabad

Approval Sheet

This thesis entitled **"Optical Properties of Graphene – Effect of Compressive Strain"** by *ManodeepMondal* is approved for the degree of Master of Science from IIT Hyderabad.
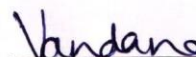
-Dr. Prem Pal-

Coordinator/Examiner
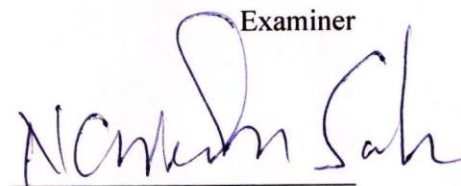
-Dr. J.Suryanarayana-

Advisor/Examiner

-Dr. J.Mohanty-

Examiner

-Dr. Vandana Sharma-

Examiner

-Dr. S.Hundi-

Examiner

-Dr. Narendra Sahu-

Examiner

Acknowledgement

I would like to express gratitude to my project supervisor Dr. J.Suryanarayana for his perpetual guidance, fervency and support throughout the project.

I sincerely thank the Department of Physics of IIT Hyderabad for providing basic infrastructure and facilities. I would like to thank Dr. Jyoti Ranjan Mohanty and all faculty members of the department for their timely assistance whenever required and encouragement. I thank Mr.M Venkatanarayana and Mr. Abhishek Talapatra for their help and guidance which helped a lot in my project. I also wish to thank research scholars Mr.A Soundaraj, Mr.Ganesh Kotnana for their constant help, encouragement and valuable suggestion during my lab work. I also like to thank my elder sister as well as research scholar Ms. Jayeeta Bhattacharjee to support me in ups and downs whenever needed during my project. I extend this opportunity also to thank all my lab mates for their cooperation. I specially remember my friends Argha, Kuntal for their love and company which I will never forget throughout my life.

I wish to express deep gratitude to my parents for their eternal love, support and encouragement.

Last but not the least I wish to thank the almighty for giving me this beautiful life so that I can enjoy his enchanting creation through the path of science.

MANODEEP MONDAL

Dedicated

To

My Parents

Abstract

Graphene is single layer of graphite with 2D honeycomb lattice (sp^2 hybridization form) shows remarkable mechanical, electrical, thermal and optical properties. It is a potential candidate for nano-electronics owing to its exotic electronic properties. However, lacking a bandgap in this semimetal is greatly narrowing its application in logic devices. Hence, it is of our interest see if we can open up band gap in graphene by applying compressive strain. For this purpose we have used a method ball milling technique to apply compressive strain. We have characterized the ball milled samples for their structural and optical properties using powder x – ray diffraction, Raman spectroscopy and UV – Vis NIR spectrometer. Using the samples which were milled at different times was used to prepare thin films. Solar cell I – V characteristics were also measured in order to find the efficiency.

From the powder x – ray diffraction technique, we could confirm that the graphene which is used for the present measurements consists of hexagonal structure and with space group $P6_3mc$. In addition to the intense reflections (002) from graphene, we also could see a peak which is related to graphene oxide (001). Hence, we believe that the properties which we would discuss will be of graphene + graphene oxide. From the Raman spectroscopy, the G peak which corresponds to breathing of sp^2 bond shifts to lower wave number which is due to compressive strain, as a result of increase in graphene layer number. Such thing can happen due to the agglomeration of graphene flakes for long milling times. D peak which corresponds to defects in graphene remains constant with respect to wave number. However, the intensity increases as a result of increase in defects. I_D/I_G ratio increases, which essentially means that the defect density increases with respect to ball milling time. 2D peak which corresponds to double phonon scattering remains constant and there is no shift for the above. Calculated band gap values from absorption spectra are in the range of 0.4 – 2.25 eV. If we think logically, as graphene is zero band gap semiconductor or semi metal, it should not give any band gap value. However, from the measurements that we performed we could see a gap opening of 0.4 eV in the parent form. What we believe is that the gap opening of 0.4 eV may have contribution from graphene oxide, which we could realize from x – ray diffraction measurements. Using these ball milled graphene we could prepare thin films on FTO substrate using drop casting method. Such films were used to measure the efficiency of solar cells. We also could see the surface morphology of films using 3D ZETA profiler and looks like the surface is smooth everywhere with the thickness of 18μm. As the ball milling time increases, the efficiency of solar cell increases from 8 x 10-5 – 1.8 x 10-3, which is the indication that band gap of graphene is varying with respect to milling time. We also have performed theoretical calculations using Gaussian 09 software, which is to calculate the

available Raman modes with respect to change in the bond angles or bond lengths. As bond length between two sp2 hybridized carbon changes, the G peak of graphene shifts to lower wave number, which is in accordance with our experimental results. However, the values of wave number don't match with respect to experimental one which could be due to the kind of structure that we have used in our simulations.

Contents

- Chapter 1 -

Introduction

We need to invest dramatically in green energy, making solar panels so cheap that everybody wants them. Nobody wanted to buy a computer in 1950, but once they got cheap, everyone bought them.
Bjorn Lomborg

Every discovery of new material shows a new era in scientific and technological research. The recent discovery of graphene-atomically thin layers of graphite- opened such an arena in science as well as technological aspects. Since the publication of the famous paper [1] on the 'sticky-tape method' for preparing graphene in October 2004 (which helped win authors, Andre Geim and Konstantin Novoselov the 2010 Nobel Prize in Physics), the field of graphene research has seen phenomenal growth. Prior to its isolation by Geim and Novoselov in 2004, it existed only in theoretical models; as such, the field of graphene research can be considered to have appeared almost overnight. Fig.1 shows how the amount of papers about graphene has exploded the last few years.
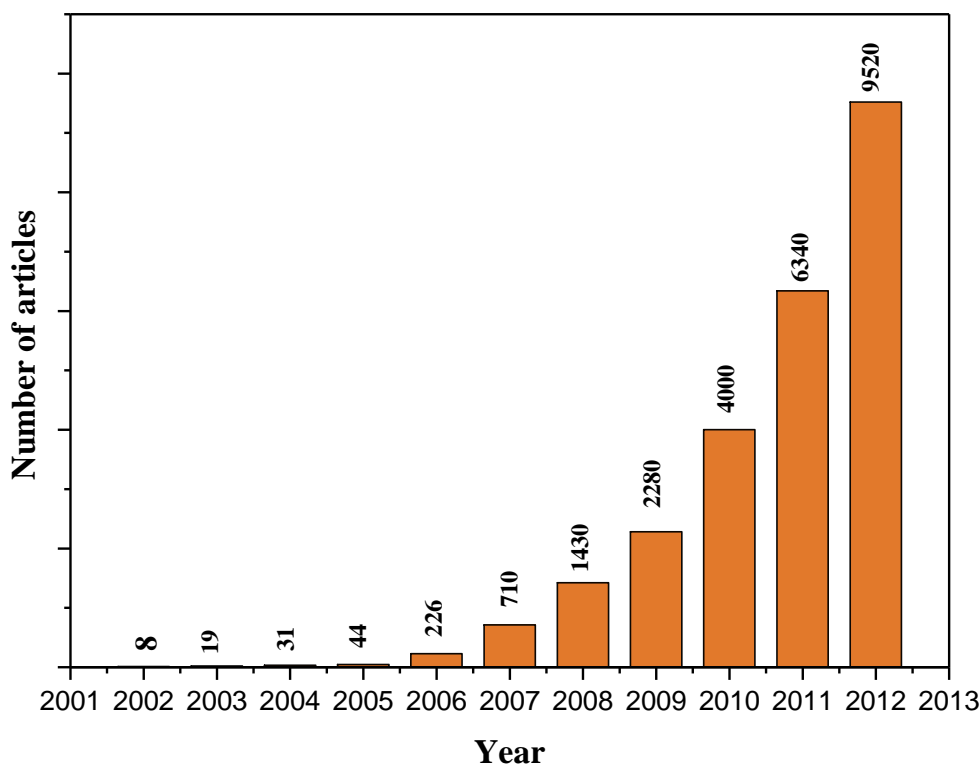
Figure 1: *Articles with "Graphene" in the title per year. Data provided by Google Scholar.*

Graphene is a purely carbon based, honeycomb structured, one atom thick layer of carbon atoms, bonded to one another by sp^2 hybridization. Its most frequent form in nature is graphite, a mere stack of graphene layers held together by Van der Waals interactions.

Graphene is discovered much later than the other carbon allotropes perhaps because the melting point of two dimensional (2D) solids is theoretically predicted to be at zero temperature according to thermodynamics. (The average vibration amplitude diverges logarithmically at any finite temperature for a 2D crystal, whereas it is convergent at any temperature for the 3D case). It remains a mystery to me how some physicist would one day come up with an idea of working on producing a material that is not supposed to exist. In any case, it is a brilliant idea now that it turns out to be possible, thanks to the courage and perseverance of the pioneers.

Despite the small thickness of graphene flakes (a couple of angstrom to a few nanometres) it display promising properties (mechanical strength and stiffness, high electron mobility[2]) that make them excellent candidate for a number of applications into Nano devices.

1.1 Motivation of the thesis:

In our modern world the day by day increasing demand for energy is totally conflicting with the increase of greenhouse gases more and more, it seems necessary and inevitable that renewable energy sources will play a major role in our future global energy system. A recent report from the Intergovernmental Panel on Climate Change says that renewable energy and Photo Voltaic will account for up to 30 % of the world's electricity production by 2050.

Solar energy is one of the most promising renewable energy sources available to us. Its abundant availability surpasses any other energy source, and over the last decade with the immense progress seen in production technology for photovoltaics (PV) we can surely say that our future generation will immensely depend on solar cell technology. Now a day the price for converting solar energy into electricity is rapidly decreasing. However, further price reductions are still required for solar energy to be directly cost competitive with conventional energy sources in the majority of the world.

Researchers all over the world are currently trying to increase the solar cell efficiency by several methods. Currently, the record efficiency of a silicon solar cell is 25% [3] , which is actually quite close to the theoretical maximum of 29 % given by the Shockley-Queisser limit. The record silicon solar cell with an efficiency of 25 % mentioned earlier is a beautiful example of solar cell engineering. The problem, however, is that in order to make such a cell; several processes that

cannot be directly transferred into mass production are employed. So our aim will be such that we can make efficient solar cell with very simple method so that everyone can meet the price of the solar cell.

.In the present situation we have 3 generation solar cells:

- **1st generation-** The first generation contains solar cells that are relatively expensive to produce, and have a low efficiency. The first generation includes cells consisting of Silicon or Germanium that are doped with Phosphorus and Boron in a pn-junction. This generation is dominating the commercial market. Silicon cells have a quite high efficiency, but very pure silicon is needed, and due to the energy-requiring process, the price is high compared to the power output.

- **2nd generation-** The second generation contains types of solar cells that have an even lower efficiency, but are much cheaper to produce, such that the cost per watt is lower than in first generation cells. Usually called thin-film solar cells because when compared to crystalline silicon based cells they are made from layers of semiconductor materials only a few micrometres thick.

- **3rd generation-** The term third generation is used about cells that are very efficient. Most technologies in this generation is not yet commercial, but there is a lot of research going on in this area. The goal is to make third generation solar cells cheap to produce. There are several technologies in this generation. One of them is Quantum Dot (QD) Solar Cells. These are built up of a semiconductor (silicon) coated with a very thin layer of quantum dots.

Graphene is a kind of novel two dimensional material and considered as a potential candidate for Nano electronics owing to its exotic electronic properties [4] However, lacking a bandgap in this semimetal greatly converging the application in logic device, and hence the modification of graphene structures for opening its bandgap is indeed a crucial step towards the practical applications in logic-device-based Nano electronics and mainly Solar Cell applications. Up to now many methods have been theoretically predicted to open bandgap in graphene, but only a few of them are experimentally proved by different research groups. Here we have surveyed some of these literatures.

- **Literature survey:**

H.Vita, S.Bottcher et al [5] investigated the hybridization of graphene and metal- derived electronic states through intercalation pseudomorphic monolayer of Cu in between graphene and Ir(111). They observed the modifications in the band structure by the intercalation process and its concomitant changes in the charge distribution at the interface. So by that method they were able to introduce a bandgap opening method in semimetal graphene.

Xiaochang Miao, Sefaattin Tongay et al [6] investigated the power conversion efficiency of 8.6% in doped graphene with bis- (trifluoromethanesulfonyl) amide which exceeds the native (undoped) device performance by a factor of 4.5 and that was the highest PCE reported for graphene-based solar cells to that time. So by the chemical doping they tried to create bandgap in graphene.

Richard Balog, Bjarke Jørgensen et al [7] reported in Nature that in graphene we can introduce bandgap by patterned hydrogen adsorption. They investigated that opening of band gap is possible in semimetal graphene through patterned hydrogen adsorption onto the Moiré super lattice positions of graphene grown on an Ir(111) substrate.

Marc Dvorak, William Oswald et al [8] showed by employing both the tight-binding modelling and first-principles electronic structure calculations that the appearance of bandgap in patterned graphene has a geometric symmetry origin. From this the analytic rule of gap-opening by patterning graphene was derived.

So there is many methods to create the bandgap on graphene but these methods are highly expensive in economical point of view so in this project my main research intention is how to create the bandgap in graphene through very simple method (Ball Milling) and to increase the efficiency of graphene based thin film solar cell and which is very cheap to produce in the large scale form. Researchers are already trying to fabricate high efficient graphene based solar cell by chemical doping method [6], here we have tried physical method(effect of stress and strain on graphene sheet) to create a band gap in semimetal graphene and to use it in thin film solar cell technology.[9]

1.2 Thesis outline:

Graphene is regarded as one of the most promising candidates for the next generation of electronic materials due to its extremely high charge carrier mobility. However, graphene lacks a band gap around the Fermi level, which is a defining feature of semiconductor materials and essential for controlling conductivity by electronic means [10]. In this project our main intention is how to create band gap in graphene by simple method so that we can use it in solar cell.

In this thesis in 2nd chapter we have written the theoretical background and properties of graphene and some simulated result that we have done.

In 3rd chapter we have discussed how we prepared the samples by Ball Milling for different times the phase purity of them was identified using powder x – ray diffraction technique. Raman spectroscopy was used to characterize the graphene. In addition, theoretical simulations were used to correlate the experimental data with the theoretically simulated data.

In 4th chapter we have given attention on optical property analysis of all samples. To characterize that we have analysed UV-Vis NIR spectroscopy graph and from that we have calculated approximate band gap of all samples using Tauc method. Then we prepared graphene thin film by drop casting method and characterized the film using 3D ZETA profiler. After that to see the solar cell efficiency of all samples we used PET solar simulator instrument and from that we got an incremental nature in efficiency with respect to milling time.

In 5th chapter we have summarised the results whatever we got from this work and we have discussed about the outlook of the project work.

- Chapter 2 -

Graphene

Graphene is a single molecule crystal of carbon atoms, forming a hexagonal "honeycomb" lattice with sp^2 hybridised bonds. Graphene refers to a single 2D plan of this crystal, while graphite is nothing but stack of layers on top of each other. In this report we will use the term Single Layer Graphene (SLG) to denote a single sheet, Double Layer Graphene (DLG) for a stack of two sheets, NLG for a stack of N graphene sheets, Few Layer Graphene (FLG) for stacks exceeding 3 layers but not more than 10 layers and Many Layer Graphene (MLG) for piles higher than 10 layers. These arbitrary limits of stacking layers are essentially based on optical observations that we will discuss in the experimental section in this thesis.

2.1 Structure:

Graphene consists of sp^2 carbon hexagonal networks, in which strong covalent bonds are formed between two adjacent carbon atoms. The unit cell for monolayer graphene (1-LG) contains two carbon atoms, A and B, each forming a triangular 2D network, but displaced from each other by the carbon–carbon distance a C–C = 0.142 nm, as shown in **Fig 2(a).** The 3D graphite structure corresponds to a stacking of the hexagonal networks of individual graphene layers in the direction perpendicular to the layer plane (c-axis) in an AB (or Bernal) stacking arrangement, in which the vacant centres of the hexagons on one layer have carbon atoms on hexagonal corner sites on the two adjacent graphene layers, as shown in **Fig 2(b).** In graphite with AB stacking, the unit cell consists of four carbon atoms A_1, A_2, B_1, and B_2 on the two layer planes shown in **Fig 2(b).** The in-plane and c-axis lattice constants for graphite are a = 0.246 nm and c = 0.670 nm, respectively. Normally, the bilayer graphene samples obtained from the mechanical exfoliation of graphite exhibit an AB stacking arrangement, and therefore the number of atoms in the unit cell of bilayer graphene (2-LG) is the same as that for graphite, with four atoms per unit cell, as shown in **Fig 2(b)** and **(c).** Tri layer graphene (3-LG) in turn contains three layers, two of which are like bilayer graphene and the third layer has atom A_3 over A_1 and atom B_3 over B_1 as shown in **Fig 2(d).** Four layer graphene (4-LG) consists of the stacking of two unit cells of the type shown in **Fig 2(c),** one stacked on top of the other.[11].
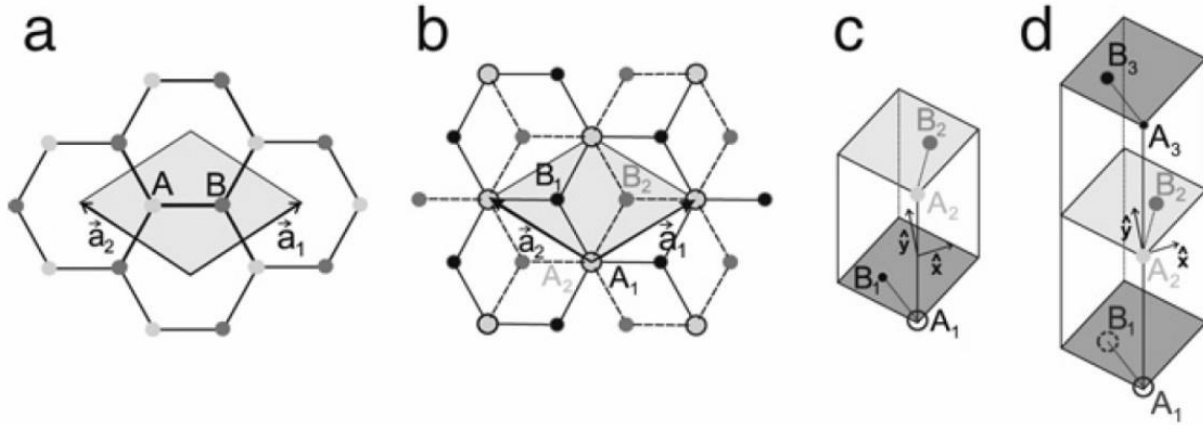
Figure 2: (a) A top view of the real space unit cell of monolayer graphene showing the inequivalent atoms A and B and unit vectors a_1 and a_2. (b) A top view of the real space of bilayer graphene. The light/dark grey dots and the black circles/black dots represent the carbon atoms in the upper and lower layers, respectively, of bilayer graphene (2-LG). (c) The unit cell and the x and y unit vectors of bilayer graphene and (d) the same as (c) but for tri layer graphene.

For carbon atom the second stable atomic arrangement is carbon bonded in a sp^2 hybridized state. Each carbon atom has 3 covalent C-C bonds of 1.42 ^0A in the x-y plane, leaving one perpendicular, dangling 2Pz orbital. This dangling bond combines with its nearest neighbours to form the π orbitals. The sp^2 covalent bonds give the graphene its mechanical strength, and the π orbitals make the graphene conducting.
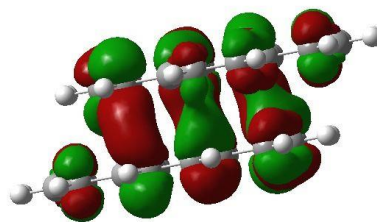
2.1.1 Theoretically simulated HOMO and LUMO:

Graphene Nano sheets have huge diversity in structure and topology, hydrogen terminated circular graphene cluster namely coronene ($C_{24}H_{12}$) was used here to simulate the structural properties and the HOMO LUMO of the two sheet graphene flake for the ease of calculation. Here we have calculated all the theoretical simulations using first principle DFT method. DFT method was implemented by GAUSSIAN 09[12] software with Beke-Lee–Yang-Parr (B3LYP) exchange – correlation hybrid function [13] and LanL2DZ [14] basis set to optimize the ground state geometry. Here all the data taken in optimized conditions. From the DFT calculations we got the charge distribution of the graphene sheets for HOMO and LUMO both. It is already reported that between the two layers of graphene sheets there is dangling 2Pz orbital and which is the responsible for graphene's too much conductivity. We have confirmed that fact by simulation as below:
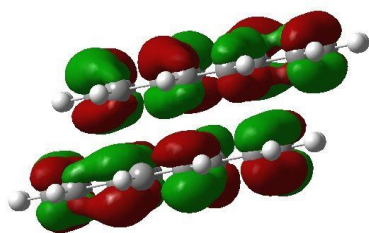
HOMO structure (Valance band)   LUMO structure (Conduction band)

Here from the simulated HOMO structure we can see that there is no overlapping between the P_z orbitals so there is no conduction between the sheets but from the LUMO we are seeing that there is a clear overlapping of two P_z orbitals and so that's why so much conductivity is there between the two layer of graphene sheets for conduction band structure.

2.2 Allotropes:

Practically from graphene we can construct all the structures made of carbon atoms from zero to three dimensions. By stacking sheets of graphene on top of each other, as shown in **Fig 3(c)**, we get graphite. The π orbitals between the different graphene layers only interact weakly, so the layers are only held together by a weak van der Waals attraction. In addition to graphite, we can imagine taking a sheet of graphene and rolling it up in to a cylinder, as shown in **Fig 3(b)**. We call these cylinders carbon nanotubes. Carbon nanotubes are the 1D cousin to graphene. Finally, if we roll a graphene sheet into a ball rather than a cylinder, as shown in **Fig 3(a),** we get a Buckminsterfullerene. Fullerenes are the 0D cousin to graphene. Here we concentrated on the single layer of graphene sheet and its properties.
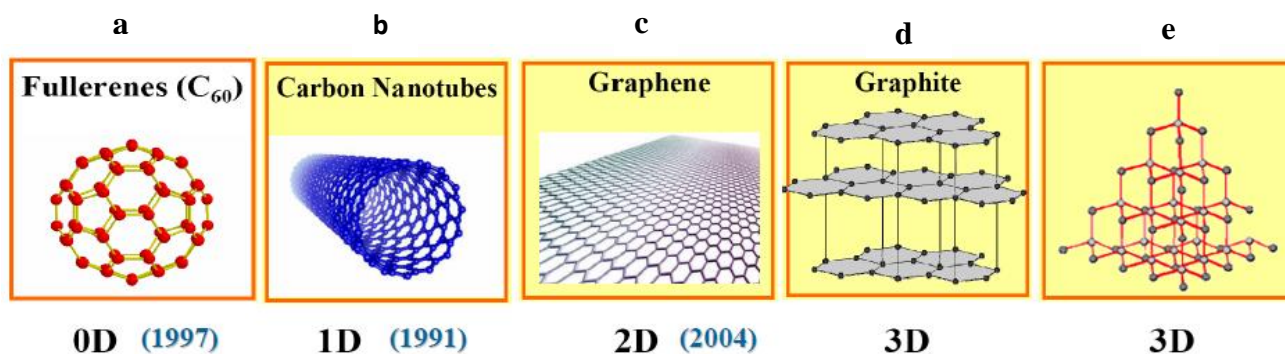
Figure 3: *(a) Schematic of how to roll up a graphene sheet to form a C-60 Buckminsterfullerene.*
(b) Schematic of how to roll up a graphene sheet to form a carbon nanotube.
(c) Single layer of graphene sheet.
(d) Schematic showing a stack of graphene sheets, also known as graphite.
(e) The 3D structure of diamond.

2.3 Properties:

2.3.1 Mechanical Properties:

In graphene sp^2 C-C bonding is the main reason for the exceptional mechanical properties of this wonder material. The static mechanical properties of an isotropic 2D membrane are described by four parameters: The in plane Young's modulus Y, the Poisson ratio v, the breaking stress σ_{int} and strain ε_{int}, and the bending rigidity B. These parameters dictate how a graphene membrane will respond to strain and deflections and determine what the frequency of NEMS (Nanoelectromechanical systems) built out of graphene will be.

The Young's modulus is defined as the relation between the linear restoring force σ_x in a membrane due to a linear (uniaxial) strain ε_x on the membrane.

$$\sigma = -Y\varepsilon_x$$

The Poisson ratio is a measure of how much a membrane contracts along a direction perpendicular to an applied (uniaxial) strain.

$$\varepsilon_y = -v\varepsilon_x$$

Experiments using AFM tips [15] showed that the Young's modulus of graphene is Y = 340 N/m. By pushing on the graphene with a diamond AFM tip [16], researchers were able to tear the graphene directly under the AFM tip. They found that the breaking stress is σ_{int}^{2D} = 42 N/m corresponding with a strain of ε = 0.25 or 25%. These measurements tell us that graphene is the strongest material on earth. Poisson's ratio v is reported with a value between 0.149 and 0.45.

2.3.2 Electronic Properties:

Graphene has been, both theoretically and experimentally, confirmed as a near perfect electronic conductor: first of all because it is zero band gap semiconductor (the conduction and valance band are touching to each other, shown in **Fig 4**) , secondly because electrons momentum k is linearly related to the energy E near the edges of the 2D first Brillouin zone. In this region the electron behaves like massless Dirac fermions and at last ballistic transport is observed in graphene sheets.
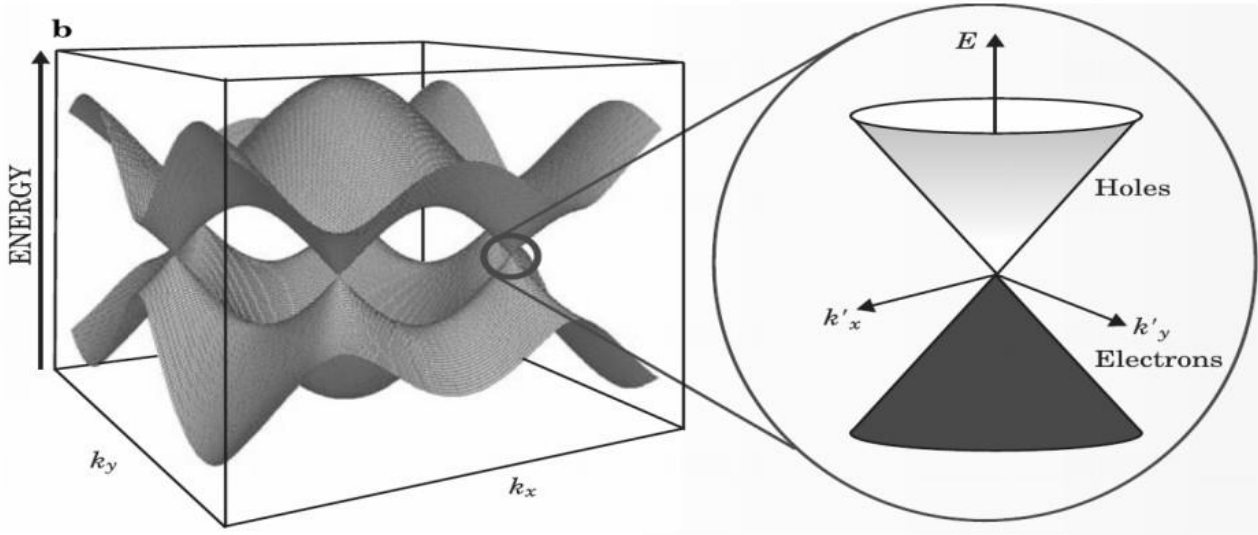
Figure 4: *Electronic band structure of graphene [11]: (left) 3D representation of a unit cell in reciprocal lattice space; (right) focus on a linear structure near a K point.*

The charge carriers at low energy are best described as massless Dirac fermions (electrons without a mass or neutrinos carrying the charge of an electron) , making them quasiparticles that can potentially undergo quantum electrodynamics (QED) phenomena. One can describe that using Dirac equations. Here is the equation below which describes the energy of the carriers:

$$E = \hbar.v_F.\sigma.k$$

Where σ the Pauli matrix, v_F the Fermi velocity, and k the quasiparticle momentum. Explicitly σ describes the pseudo-spin of the quasiparticle, and k is chirality.

In a normal conductor the charge carriers (either electrons or holes) are scattered during their movement through the material and by that they are dissipating their momentum. In graphene however the charge carriers can travel as far as 0.3 μm [2] without being scattered: that is called ballistic transport. The conduction and valence bands of graphene meet at 6 points in k-space known as the Dirac points. Near the Dirac points, the band structure disperses linearly as cones with slope of the energy written earlier, where Fermi velocity in 10^6 m/s. At the Dirac point, the density of states goes to zero and the conductivity should go to zero as well. However, at these low densities, the electrons start experiencing long-range, many-body interactions not captured by the tight-binding model [17].

2.3.3 Optical Properties:

The unusual band structure of graphene also affects how it interacts with light. The optical absorption A of graphene follows a surprisingly simple relation.

$$A = \pi.\alpha = 2.3\ \%$$

Where $\alpha = 1/137$ is the fine structure constant. By measuring the intensity of light we can see that each layer of graphene absorbs 2.3% of light. This strong interaction with light of even a single layer of atoms is what makes graphene visible on a silicon chip, and also allows us to perform opt mechanical resonance measurements.

Below we have mentioned all the properties of pristine graphene as a chart form:

Table: Properties of Pristine Graphene		
C-C bond length	d	$1.42\ A^o$
Graphite interlayer distance	t	$3.42\ A^o$
Fermi Velocity	v_F	10^6 m/s
Typical mobility	μ	1000 - 20,000 cm^2/Vs
Optical absorbance (per layer)	A	2.29 %
Poisson ratio	υ	0.17
Breaking stress	σ_{max}	42 ± 5 N/m
Breaking strain	ε_{max}	0.25

2.4 Synthesis:

Several methods for preparing graphene have been reported. And with the advancement of the research new methods are reporting for the mass production of graphene flakes. Here we have mentioned some processes to produce high quality of graphene.

2.4.1 Mechanical Exfoliation:

In this method we will use highly oriented pyrolytic graphene (HPOG) as a precursor. In this method we use a piece of cellophane tape to draw a thin film from highly oriented pyrolytic graphite. After repeated peeling from the thin film, it is ultimately stamped onto a substrate and the tapes are carefully amputated. The deposition formed is a dense network of single and multi-layered graphene, which is cleansed before using for specific purpose.

2.4.2 Thermal Decomposition of SiC:

The thermal decomposition of silicon carbide is a technique that consists of heating SiC in ultra-high vacuum (UHV) to temperatures between 1000∘C and 1500∘C. This causes Si to sublimate from the material and leave behind a carbon-rich surface. Low-energy electron microscopy (LEEM) studies indicate that this carbon layer is graphitic in nature, which suggests that the technique could be used to form graphene [18]. The Si face of a 6H-SiC single crystal was first prepared by oxidation. The sample was then heated by electron bombardment in UHV to 1000∘C to remove the oxide layer. Once the oxide was removed, the samples were heated to 1250–1450∘C, resulting in the formation of thin graphitic layers. Typically, between 1 and 3 layers were formed depending on the decomposition temperature.

2.4.3 Chemical Vapour Deposition:

In contrast to the thermal decomposition of SiC, where carbon is already present in the substrate, in chemical vapour deposition (CVD), carbon supplied in gas form and a metal is used as both catalyst and substrate to grow the graphene layer. Two kinds of substrate are generally sued for production of graphene by this method as discussed below.

- **Growth on Nickel:**

Yu et al. grew few-layer graphene sheets on polycrystalline Ni foils. The foils were first annealed in hydrogen and then exposed to a CH_4-Ar-H_2 environment at atmospheric pressure for 20 minutes at a temperature of 1000◦C. The foils were then cooled at different rates between 20°C/s and 0.1°C/s. The thickness of the graphene layers was found to be dependent on the cooling rate, with few layer graphene (typically 3-4 layers) being produced with a cooling rate of 10◦C/s. Faster cooling rates result in thicker graphite layers, whereas slower cooling prevents carbon from segregating to the surface of the Ni foil [19].

- **Growth on Copper:**

Li et al. used a similar process to produce large-scale monolayer graphene on copper foils. 25μm thick copper foils were first heated to 1000◦C in a flow of 2 sccm (standard cubic centimetres per minute) hydrogen at low pressure and then exposed to methane flow of 35 sccm and pressure of 500 mTorr. Raman spectroscopy and SEM imaging confirm the graphene to be primarily monolayer independent of growth time. This indicates that the process is surface mediated and self-limiting [20].

2.4.4 Molecular Beam Deposition:

Zhan et al. succeeded in layer-by-layer growth of graphene using a molecular beam deposition technique. Starting with an ethylene gas source, gas was broken down at 1200◦C using a thermal cracker and deposited on a nickel substrate. Large-area, high-quality graphene layers were produced at 800◦C. This technique is capable of forming one layer on top of another, allowing for synthesis of one to several layers of graphene. The number of graphene layers produced was found to be independent of cooling rate, indicating that carbon was not absorbed into the bulk of the Ni as in CVD growth on nickel [21].

2.4.5 Unzipping Carbon Nanotubes:

Multiwalled carbon nanotubes were cut longitudinally by first suspending them in sulphuric acid and then treating them with KMnO4. This produced oxidized graphene nanoribbons which were subsequently reduced chemically. The resulting graphene nanoribbons were found to be conducting, but electronically inferior to large-scale graphene sheets due to the presence of oxygen defect sites [22].

2.4.6 Sodium-Ethanol Pyrolysis:

Graphene was produced by heating sodium and ethanol at a 1:1 molar ratio in a sealed vessel. The product of this reaction is then pyrolized to produce a material consisting of fused graphene sheets, which can then be released by sonication. This yielded graphene sheets with dimensions of up to 10 μm [23].

For our experimental purpose we have used commercially available graphene Nano powders from Redex Technologies Pvt. Ltd. and where they produced graphene by CVD method. The used graphene samples have overall thickness of 3 nm. and specific gravity 2gm/cc.

- Chapter 3 -

Structural Analysis

Commercially available graphene is used for all of our measurements from Redex Technology Pvt. Limited. At first we have done Ball Milling of the graphene sheets for different times the phase purity of them was identified using powder x – ray diffraction technique. Raman spectroscopy was used to characterize the graphene. In addition, theoretical simulations are used to correlate the experimental data with the theoretically simulated data.

3.1 Ball Milling of Graphene:

We have ball milled all the graphene samples for different times using the Retsch PM100 Planetary Ball Mill equipment. During the ball milling we are essentially applying strain and stress on the graphene sheets. Our primary aim is to apply compressive strain on graphene which would eventually change the bond angles or lengths, consequently opens the bandgap. In the figure given below we have tried to show how the balls give pressure on the graphene sheets.
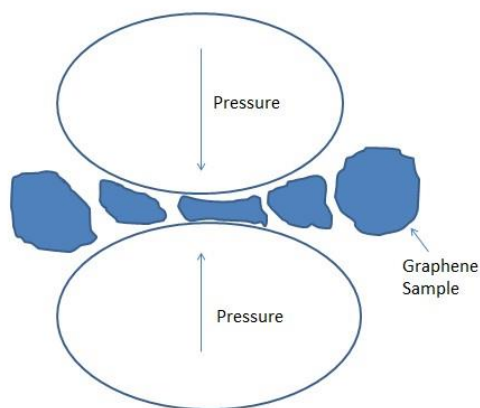
Figure 5: *A schematic diagram of how pressure is given on graphene samples by ball milling method by tungsten carbide balls.*

We have done ball milling of the graphene samples for six times for different times, say: 15min 30min 45min 1hr 1.5hr and 2hr respectively. Sample was collected between each and every interval in order to study structural, and optical properties. Ball to powder ratio that was used is 1:10. Below are the parameters that we used to mill graphene:

Sample Weight	0.15 gram
1 Ball Weight	0.2073 gram
No. of Balls	8 each time milling.
Medium	Toluene
Rotation per minute.	400

After ball milling all the samples we dried from Toluene and kept it respective containers. Here after that all the samples have been characterized by different methods as discussed below.

3.2   Structural Characterization:

3.2.1 XRD spectra Characterization:

To know the crystal structure we have done the powder x-ray diffraction and analyzed all the peaks. XRD pattern gives the size and shape of the unit cells and atomic positions within the unit cells. X-ray diffraction scans of all ball milled and parent graphene flakes were performed with Bruker's advanced X-ray diffractometer using CuKα radiation of wavelength 1.5418 ^{0}A and each sample was scanned for 1 hour with step size 0.01 degree. The basic principle of XRD is Bragg's Law of diffraction as follows.

$$2d_{(hkl)} \sin \theta = n\lambda$$

Where, $d^2 = \frac{a^2}{(h^2+k^2+l^2)}$ and a = lattice parameter.
θ = angle between the two rays.
n = number of orders.
λ = wavelength of the incident ray.

We have plotted the graph between the 2θ vs. Intensity of all the samples and from there we calculated the lattice parameter and the d spacing of the samples. We could see that structurally not much change is observed upon milling time.

The XRD plots are given below:
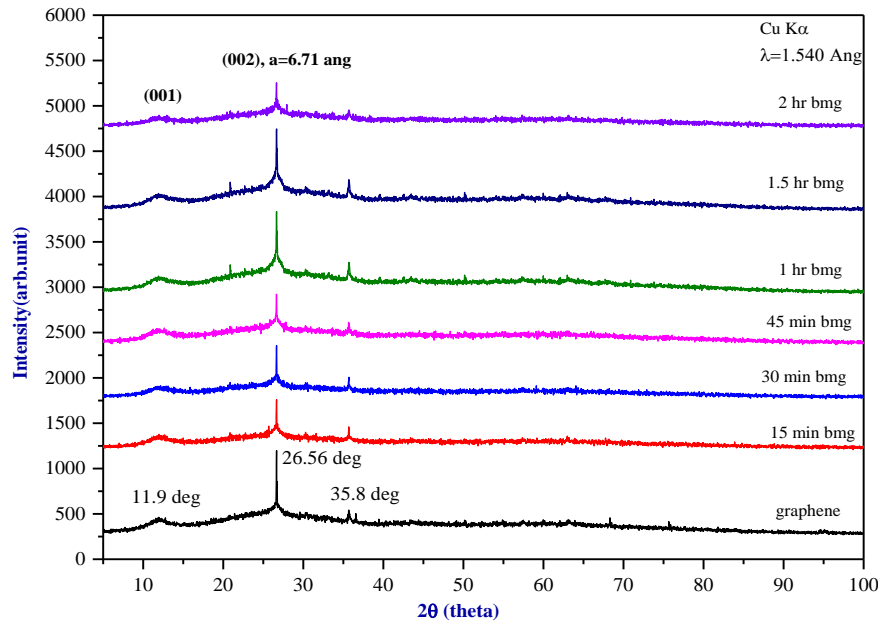
Figure 7: *XRD pattern of all ball milled samples with respect to milling time.*

In the XRD pattern of graphene samples the main graphene peak is 2θ equal to 26.56 degree peak and other two peaks are respectively 11.9 degree and 35.8 degree which corresponds to graphene oxide (GO) .

3.2.1(a) Crystallite size determination by XRD spectra:

X-ray diffraction is one of the surest methods to determine the size of the Nano crystalline powders using the very famous Scherrer formula: [24]

$$L = \frac{K\lambda}{\beta.\cos\theta}$$

Where, K = constant related to crystallite shape, normally taken as 1.84.[25].

λ = X-ray wavelength in nm.

β = peak width of the diffraction peak profile at FWHM.

θ = angle at which the main peak formed.

Here we are using CuKα radiation source of wavelength 0.15418 nm. So all the calculation is done taking λ = 0.1540 nm and K = 1.84. Using the above relation we have seen that a gradual decrease in

crystallite size with respect increase in ball milling time. The given chart below corresponds to all the value of different ball milling samples:

Sample	FWHM value (β)	Crystallite size (nm)
Parent	0.057	5.10
15 min. BMG	0.0606	4.80
30 min. BMG	0.0666	4.37
45 min. BMG	0.07126	4.06
60 min. BMG	0.0852	3.41
90 min. BMG	0.0937	3.10
120 min BMG	0.1039	2.80

Now here we have plotted the ball milling time vs. Nano crystallite size graph and from there it is confirmed that gradual decrement in crystallite size occurs but there exists no structural change.
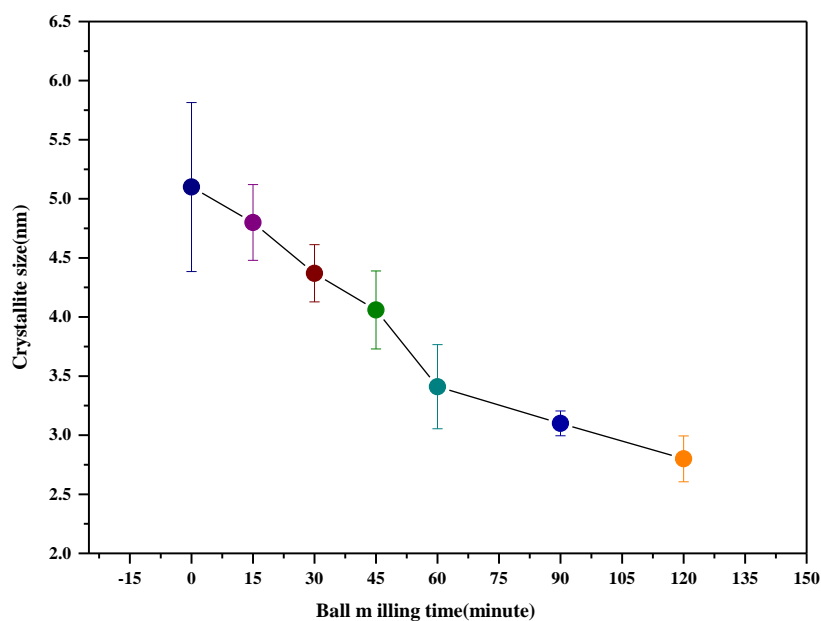

Figure 8: *Gradual decrement in crystallite size with respect to increase in milling time.*

3.2.2 Raman spectra characterization:

For graphene material identification and characterization Raman spectroscopy is the surest one. From this we can characterize those samples also which are under strain. Prof. C.V Raman was awarded Nobel Prize in Physics in 1930 for his remarkable discovery.

When the sample is irradiated by a monochromatic beam then the interaction occurs with beam and the molecules of the sample. By this the sample can be somehow perturbed or altered by the radiation and it can be absorbed, reflected, diffracted, or scattered. For the scattering process to possible condition can be appeared, the incident beam will scatter elastically or inelastically. The former scattering process is called the Rayleigh scattering and which is responsible for most of the scattered beam while the latter is called Raman scattering and which is responsible for less than 10^{-5} of scattered intensity.

Raman's scattering gives the information about the vibrational and rotational states of the molecules. For Raman scattering monochromatic and coherent Laser light beam is used. The inelastic Raman scattered radiation can correspond either excitations of the sample's phonons (Forming of Raman Stokes lines) or to their relaxation (Forming Raman Anti Stokes lines).
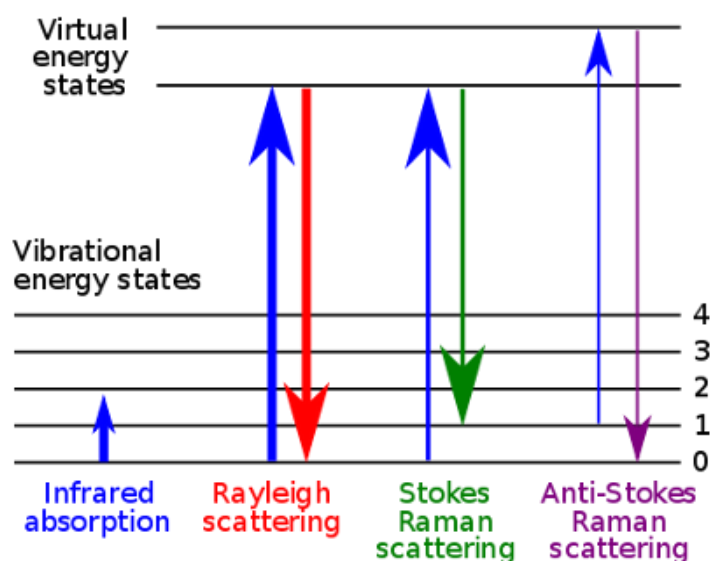
Figure 9: *Schematic view of Raman's scattering process and Stokes and Anti Stokes line formation.*

Now in the present work we have taken the Raman spectrum of different hour ball milled graphene samples to see the vibrational modes of the graphene and how it is changing with respect to ball
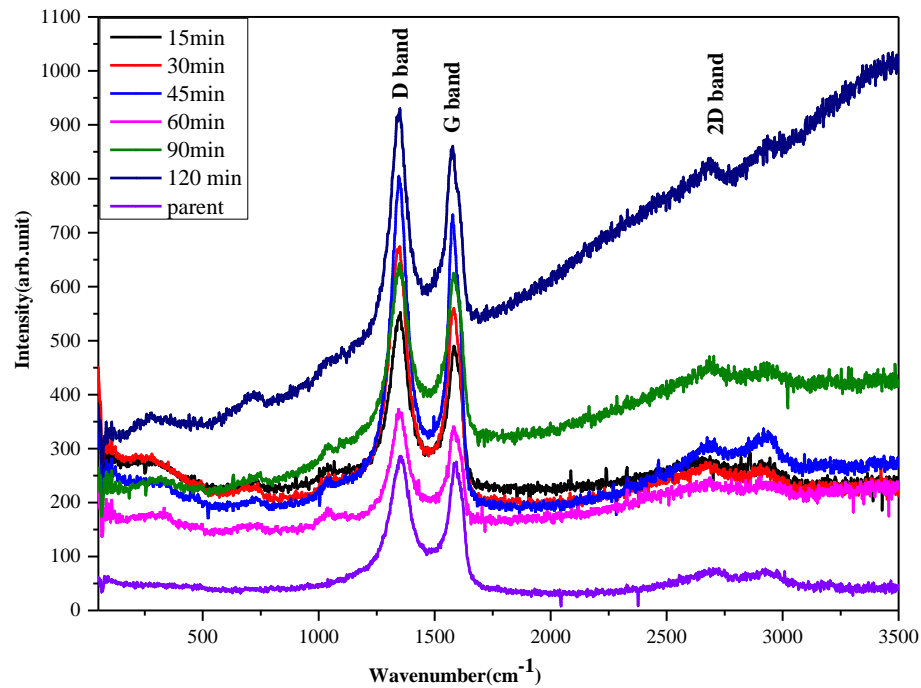
milling time. For our purpose we took Raman spectrum from PerkinElmer Raman Spectrometer setup using the following conditions:

Laser wavelength (λ) = 532 nm.
Power = 20 mW.
Integration time = 20 sec.
Lenses used = 100x.

Figure 10: *Raman spectrum of all ball milled and parent samples with 532 nm excitation Laser.*

A great deal of detail on the fine structure of graphene can be extracted from the Raman spectrum. At a glance we can say that the Raman spectrum of graphene is consist of two major bands and only few some other bands. Two main bands in this spectrum are known as G band at 1582 cm^{-1} and the 2D band at 2685 cm^{-1}. A third band known ad D band at 1350 cm^{-1} is also worth some discussion. Now we will take closer at each of these bands.

3.2.2 (a) The G band:

- **Experimental view point:**

The G band is the main first order Raman band in graphene which is doubly degenerate in-plane sp^2 C-C stretching mode [26]. This band represents the planar configuration of the graphene sheet. The G band originates from phonons at the Γ point in the centre of the first Brillouin zone. The G band comes into picture from an incident photon that resonantly excites a virtual electron–hole pair in the graphene. Then the electron or the hole are scattered by the phonon. The electron–hole pair then radiatively re-combines and emits a photon that is red shifted by the amount of energy given to the phonon [26].

From G band we can calculate the number of layer of a graphene sheet. The most important thing that we can say from the G band shifting is that external stress or strain effect on the graphene sheets. In our case also due to ball milling the shifting in G band is seen and in the coming section I will discuss about that in experimental and theatrical basis.

For G band here it is shown that how the band is shifting toward lower wavenumber with respect to increase in ball milling time:
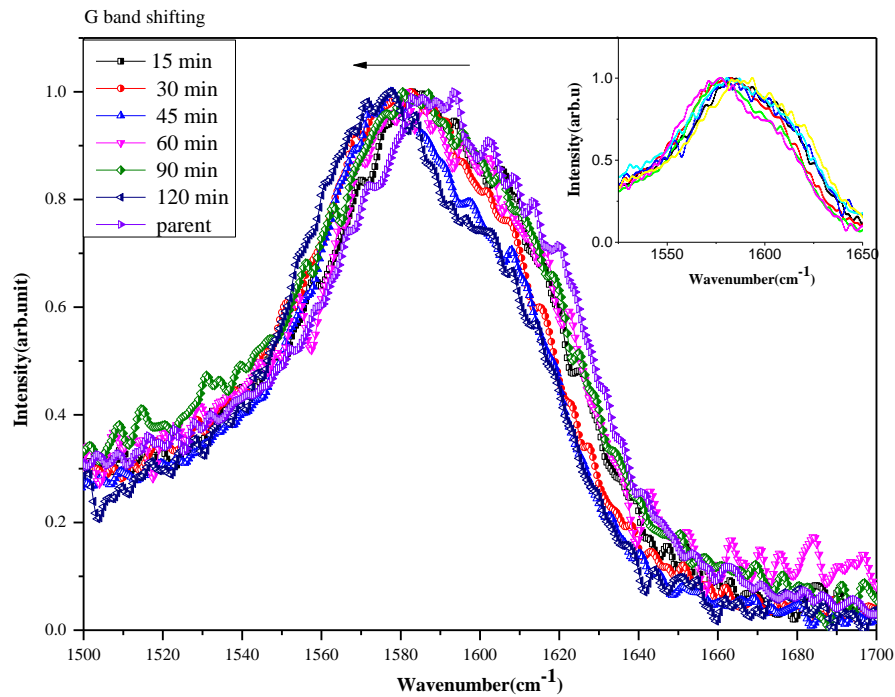
Figure 11: *Raman G band shifting of graphene to lower wave number with respect to increase in milling time.*

Here we have plotted the graph between milling time vs. G band shifting to realize the fact how it is decreasing with respect to milling time.
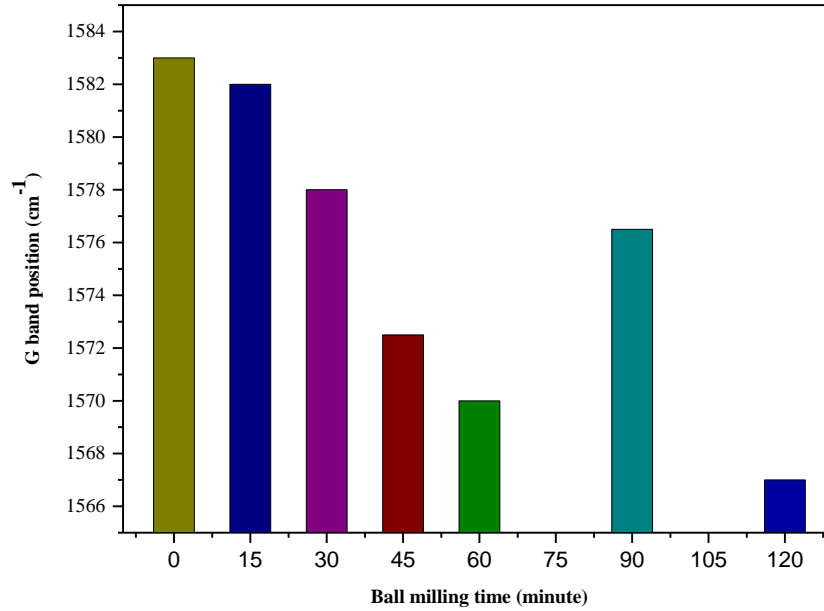

Figure 12: *Graphical representation how the Raman G peak is shifting towards lower wavenumber with increase in milling time.*

It is already published in that if we give external stress or strain on the graphene sheets then the G band will go lower or higher wave number according to what kind of stress or strain we are applying. Due to positive or negative strain the G band splits into two components which have been termed G^- and G^+ [27] . The most stunning feature is that we can say from the analysis that if splitting of G peak to G^+ and G^- is gradually goes to lower wave number then compressive strain acts as dominant part but if it is going to higher wavenumber then repulsive stress is playing major role [28]. In our plotted graph the G peak is going to lower wave number so by ball milling as if we have created strain on the graphene sheets and by this method we will see in the following chapter that there is a gradual formation of band gap in the zero band gap semi metal graphene.

- **Theoretical view point:**

We have done theoretical simulation to show that how the compressive strain plays a major role in the G band shifting. All the DFT calculation was implemented by GAUSSIAN 09[12] software with Beke-Lee–Yang-Parr (B3LYP) exchange–correlation hybrid function [13] and LanL2DZ [14] basis set to optimize the ground state geometry as well as to compute the theoretical vibrational spectrum and how the electron density (HOMO & LUMO) is changing on the graphene sheet with the compressive strain acting on the bonds. For the simplicity we have done all the calculation using one sheet of graphene with 24 Carbon atoms as shown below:
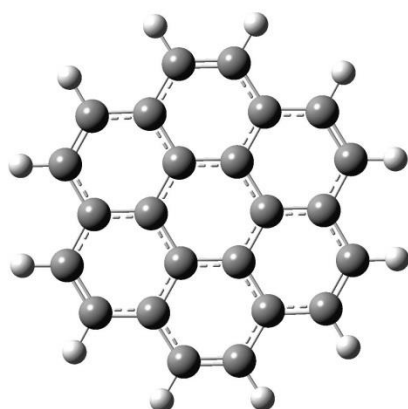

Figure 13: *24 Carbon atoms containing Graphene Nano flakes taken as standard simulation material.*

For the theoretical confirmation of G band shifting due to strain in the bonds we have changed the bond length of particular Carbon atoms in particular site. Then taking the graphene sheet as neutral (charge 0) and it is in singlet state we have computed the theoretical Raman spectra by using GAUSSSUM 2.2 software [29]. The entire Raman plot is taken by setting ambient condition at 532 nm excitation Laser wavelengths and 300 kelvin temperature. After that using GAUSSIAN 09 software we have calculated how the electron density is changing when the atomic distance is changing.
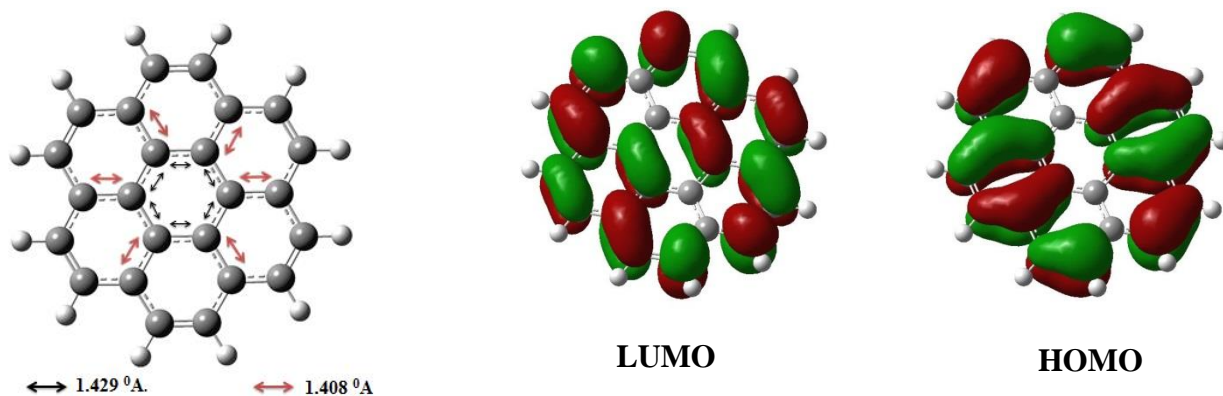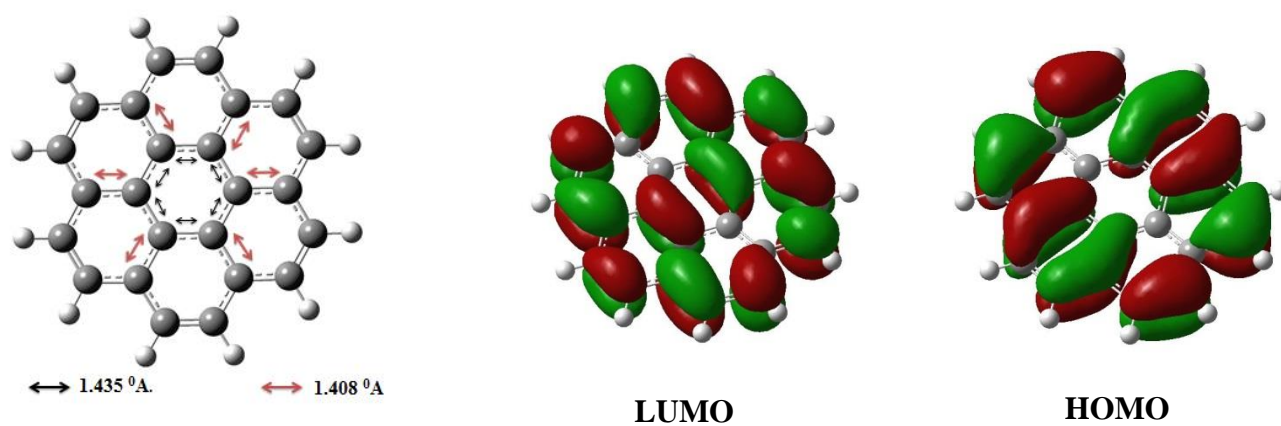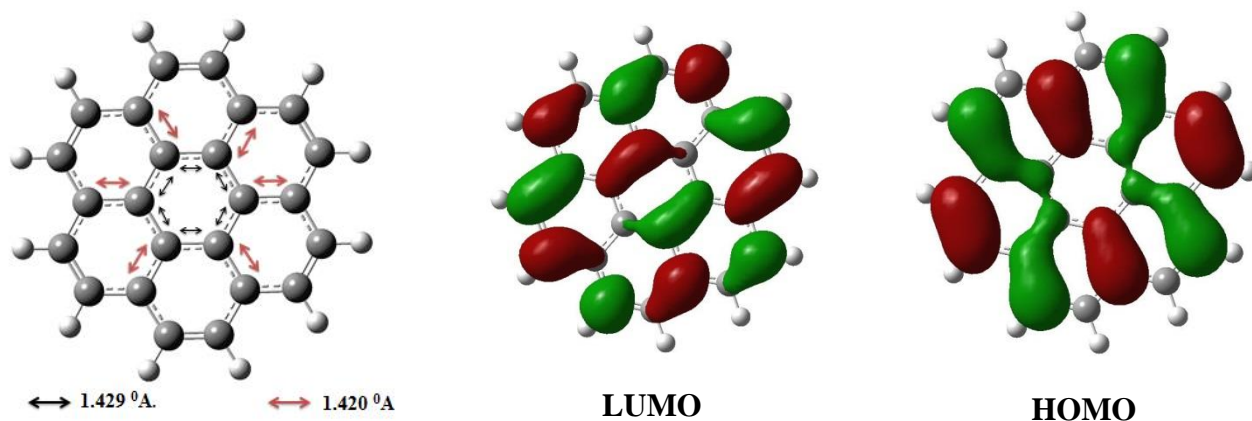
Figure 14(a): *Structure of Parent graphene sample and HOMO LUMO structure.*
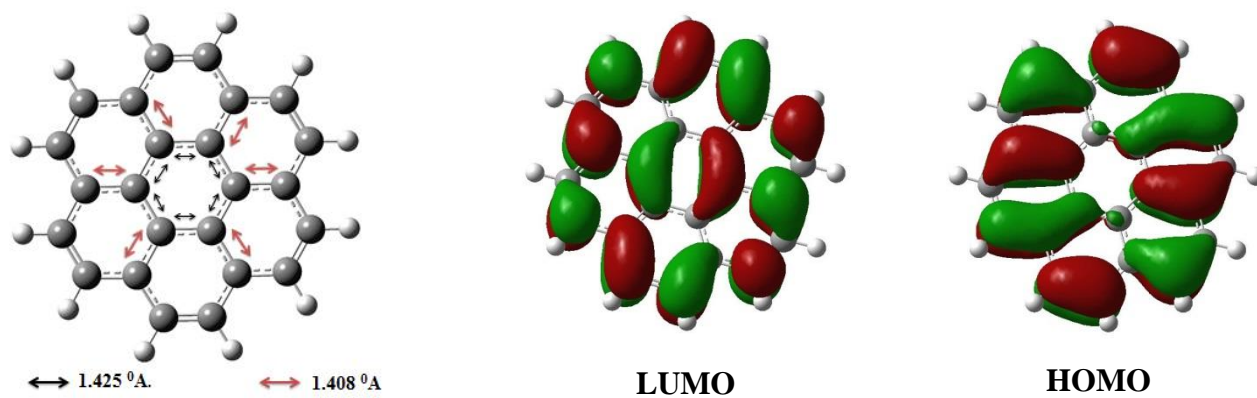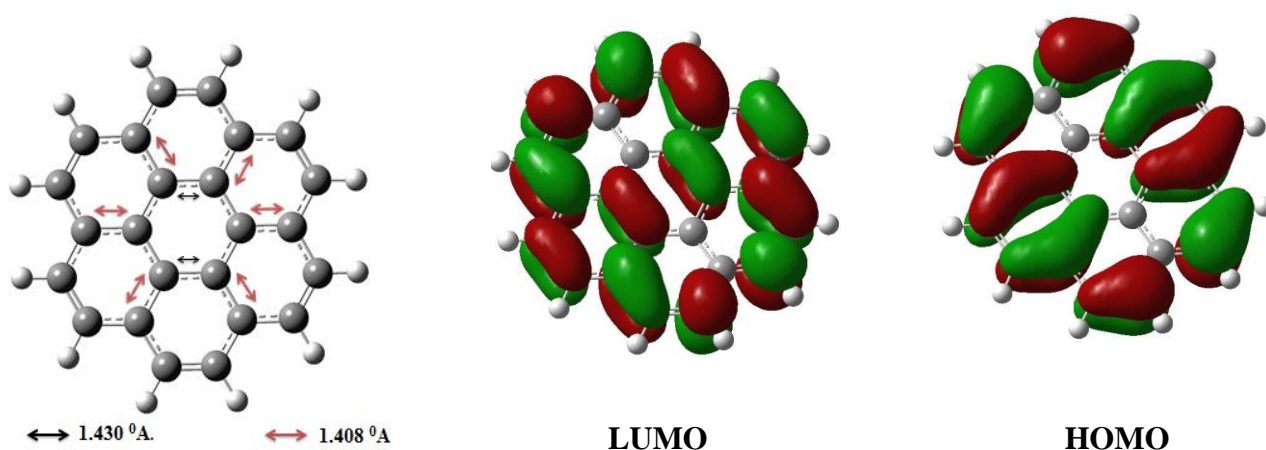

Figure 14(b): *Structure of disordered (1) graphene sample and HOMO LUMO structure.*

Figure 14(c): *Structure of disordered (2) graphene sample and HOMO LUMO structure.*

$\longleftrightarrow$ 1.429 ^{0}A. $\longleftrightarrow$ 1.420 ^{0}A   LUMO   HOMO

Figure 14(d): *Structure of disordered (3) graphene sample and HOMO LUMO structure.*

$\longleftrightarrow$ 1.430 ^{0}A. $\longleftrightarrow$ 1.408 ^{0}A   LUMO   HOMO

Figure 14(e): *Structure of disordered (4) graphene sample and HOMO LUMO structure.*

So here we could see that for the parent compound the graphene sheet is in stable condition where bond lengths are 1.429 ^{0}A and 1.408 ^{0}A respectively. Now when we distort the structure by changing some amount in the bond distance then the electrons also delocalizing and HOMO LUMO structure changes accordingly.

Now from the theoretical Raman spectrum data we have plotted the G band separately and from there also we can see that for the compressive strain on the graphene sheet the G band is going to lower wavenumber and when there is tensile strain on the sheet then the G band is shifted to higher wave number. As we could see there is a change in the wave number for experiment and theory which could be due to the kind of structure that I chose in simulation:
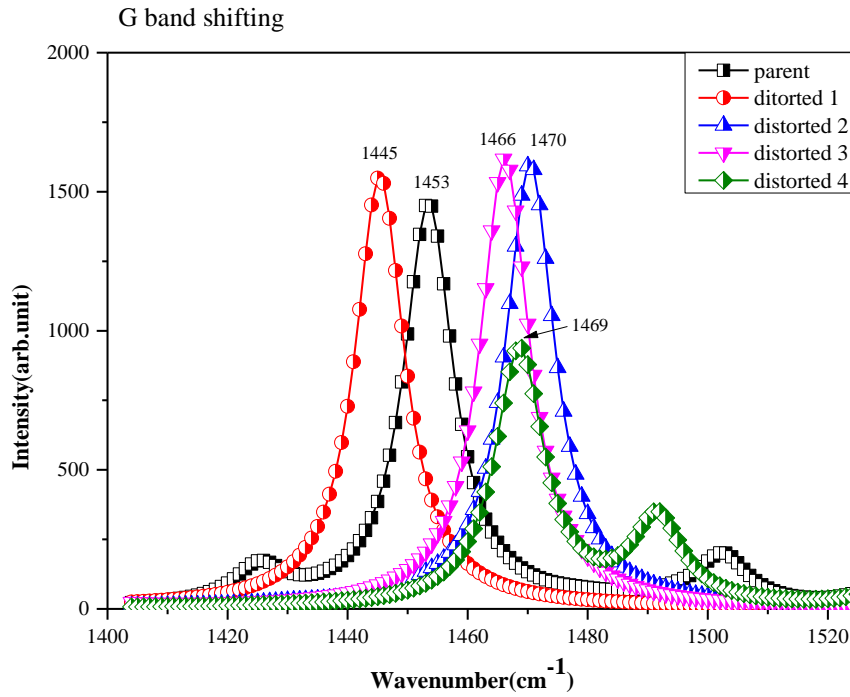
Figure 15: *Theoretical Raman spectra of G band and the shifting of G band with increase in compressive and tensile strain on graphene sheet.*

3.2.2 (b) The D band:

The D-band is known as the disorder band or the defect band. The breathing mode from sp^2 carbon rings is represented by the D band. The D band originates from the result of a one phonon lattice vibrational process. The band is typically very weak in graphite and is typically weak in graphene as well. For significant D-band it indicates that there are a lot of defects in the material. The intensity of the D-band is directly proportional to the level of defects in the sample. Another thing is that the D-band is that it is a resonant band that exhibits dispersive behavior. This means that there are a number of very weak modes underlying this band and the choice of excitation laser used will enhance different modes. The consequence of this is that both the position and the shape of the band can vary significantly with different excitation laser frequencies, making it is important to use the same excitation laser frequency for all measurements when characterizing the D-band.

For our experimental procedure we can see that there is no shifting of the D band but the $\frac{I(D)}{I(G)}$ is increasing linearly with the increase in milling time. So from that we can confirm that the defect is increasing in the graphene sheet with increase in milling time.
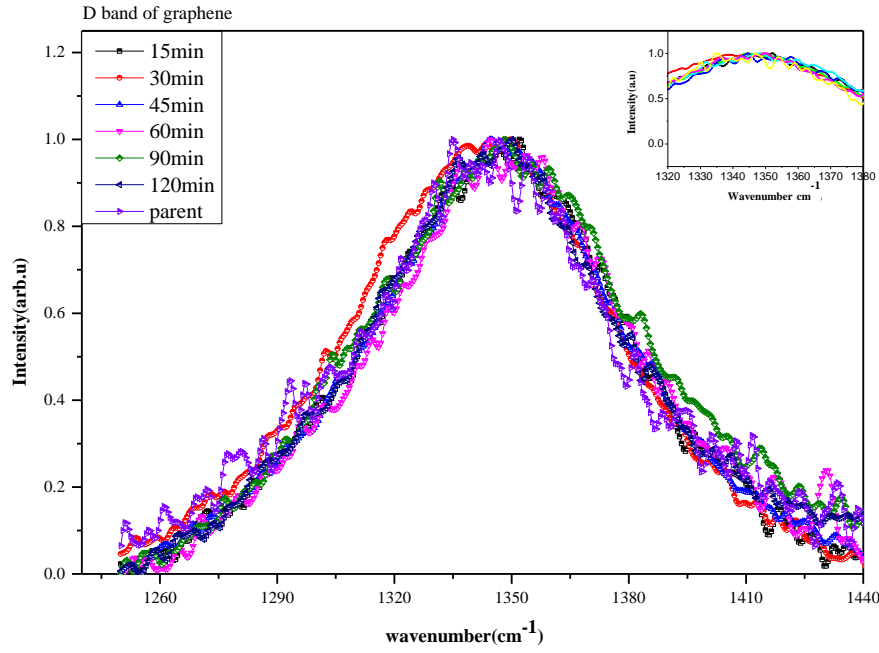
Figure 16: *D band of all ball milled samples and no shifting is there.*

3.2.2 (c) The 2D band:

2D band is sometimes referred to as the G′-band. The 2D-band is the second order of the D-band, sometimes referred to as an overtone of the D-band. It is the result of a two phonon lattice vibrational process, but unlike the D-band, it does not represent the defect on the graphene sheet. As a result the 2D-band is always a strong band in graphene even when no D-band is present, and it does not represent defects. This band is also used when trying to determine graphene layer thickness; however the differences between single and bilayer graphene in this band are more complex than a simple band shift, as was observed with the G-band. 2D-band is very sensitive to graphene folding, which needs to be considered when trying to use this band to determine layer thickness in graphene samples.

3.2.2 (d) Crystallite size determination by Raman spectra:

From Raman spectra we can determine the crystallite size as we determined from the XRD spectra. Tuinstra and Koenig studied about the Raman spectra of graphite [30] and they confirmed from their study that I(D)/I(G) varies inversely with the crystal size L_a, in their reported work they have concluded one empirical formula to calculate the crystal size as:

$$L_a = 4.4 * \left(\frac{I(D)}{I(G)}\right)^{-1} nm$$

Where, I(D) = Intensity of D peak.

I(G) = Intensity of G peak.

L_a = Size of crystallite in nanometer.

Now implementing this formula we have calculated the crystallite size as below:

Sample	Crystallite size(nm)
Parent	4.4
15 min. BMG	4.2
30 min. BMG	3.83
45 min. BMG	4.51
60 min. BMG	4.2
90 min. BMG	4.85
120 min. BMG	3.82

So from the above calculated crystallite size and the calculated crystallite size from XRD data if we compare we can see that the average crystallite size in not more than 5 nm and there is decrease in size with respect to increase in ball milling time.

- Chapter 4 -

Optical Property Analysis

Optical properties of graphene were carried out using commercially available graphene sheets from Redex Technology Pvt. Limited. In this chapter we will concentrate on the optical properties of different ball milled samples and band gap measurement from the UV-Vis NIR spectra and we also we would like to focus on the solar cell efficiency of thin films of graphene which were prepared using drop casting method.

4.1 Characterization:

4.1.1 UV-Vis NIR Spectroscopy:

Using UV – Vis NIR spectrometer, we essentially collected the data pertinent to the transmission or absorption of graphene sheets which were dispersed in deionized water. UV-Vis NIR Spectrometer acts on the principle of Beer-Lamberts law:

$$A * \log_{10}\left(\frac{I_0}{I}\right) = \epsilon * C * L$$

A= Measured Absorbance.

I_0= Intensity of the Incident light.

I= Intensity after transmission.

ϵ= Extinction Coefficient.

C= Concentration of the sample.

L= Length of the container.

For our experiment we used PerkinElmer UV-Vis NIR spectrometer in the range of scan 200nm to 800nm. When the light passes through the sample molecules which exists in sample absorbs the light at various wavelengths depending upon nature of the bonding of that particular molecule. The origin of the absorption can be described by the nature of the valance electrons. The valance electron can generally be found in three types of orbitals as single or σ bonding orbitals, double or triple π bonding orbitals and non-bonding lone pair orbitals. Now σ bonding orbitals is lower in energy than π bonding orbitals and π bonding orbitals are lower in energy than non-bonding orbitals. So in

correct frequency the transition occurs from these orbitals to empty orbitals mostly in anti-bonding orbitals σ^* and π^*. In the figure below that transition is shown.
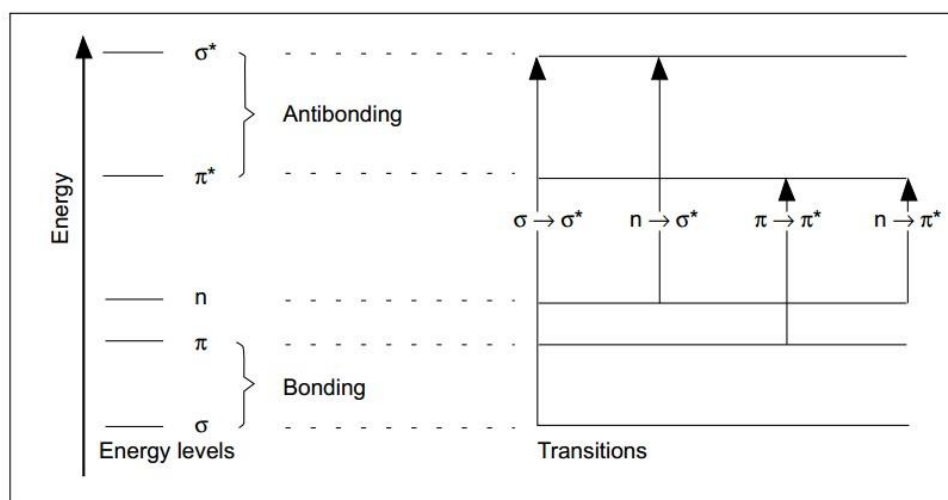
Figure 6: *Electronic transition in UV-Vis spectroscopy.*

UV-Vis NIR spectroscopy of different hour ball milled graphene samples.

Graphene samples are ball milled in Toluene medium using *tungsten carbide* balls.

⬇

Different hour ball milled samples then sonicated using probe type sonicator.

⬇

Sonication details:

Time -Each sample 25 min.
Temp - 60 degree.
Sample Amount - 0.0054 gm.
DI water medium - 40 millilitres
Resting Time -10 sec.

⬇

For every sample immediately after sonication has been taken UV-Vis NIR spectroscopy.

After taking UV-Vis NIR data of all the samples we have plotted graph of absorbance vs wavelength of all the ball milled samples. From the plot we have analyzed if any band gap formed during the ball milling of the samples with different time scales. In the result and discussion section we have discussed the band formation of graphene samples through ball milling. Here below we show the plot between absorbance vs wavelength.
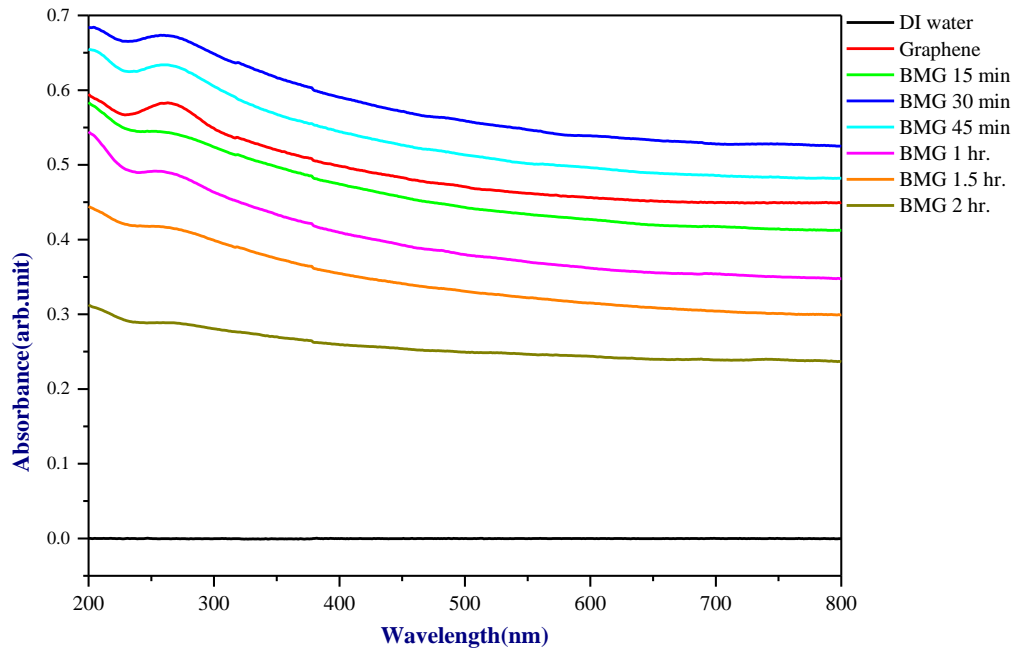

Figure 17: *Absorbance vs wavelength plots of different hour ball milled samples in UV-Vis NIR spectrometer.*

• **Band gap calculation from UV-Vis NIR spectra:**

To calculate the band gap from the UV-Vis plot we have done some graphical method which has already been published on graphene oxide band gap measurements. To calculate the optical bandgap we have used Tauc plot with a linear extrapolation [31]. As in the graphene UV-Vis spectra there is no sharp peak of absorption so we have used this method. Essentially From this method we could get the range for optical bandgap where the optical band gap resides. As in our calculated Tauc plot it is very difficult to identify the linear region of the plot so approximately we have measured the bandgap from linear extrapolation.
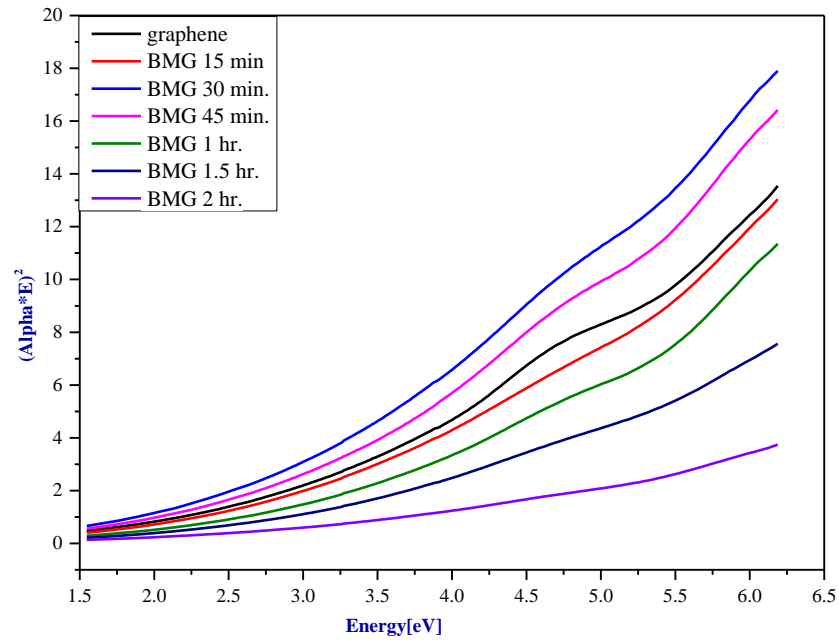
Figure 18: *Tauc plot of all graphene samples*

Now individual Tauc plot is shown for all graphene samples and from there by linear extrapolation we have calculated the optical bandgap for all the samples:
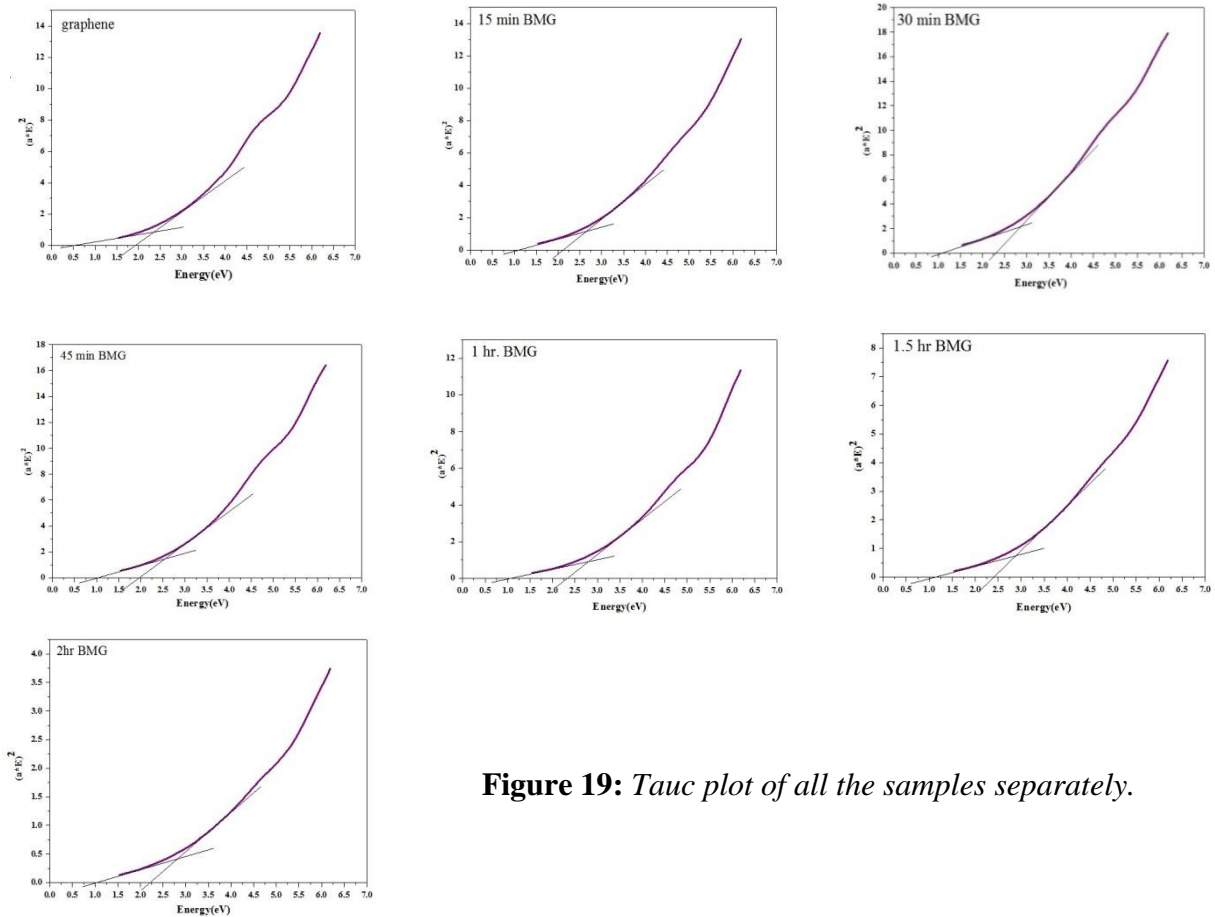
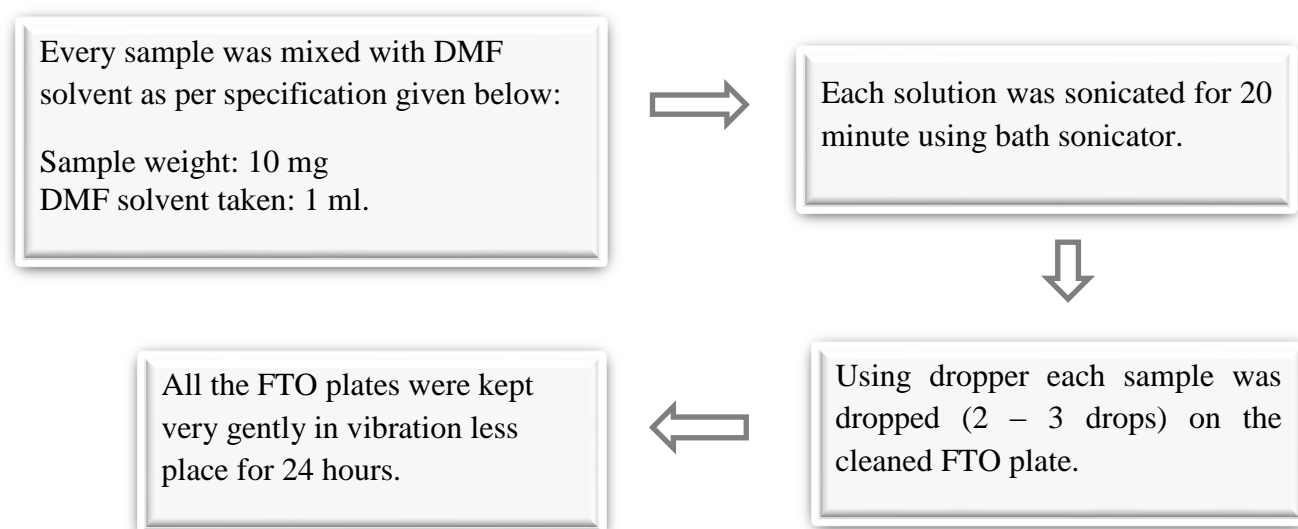**Figure 19:** *Tauc plot of all the samples separately.*

From the linear extrapolation, we could calculate the optical band gap for different ball milled samples. The bandgap values for all samples are given below in tabular form:

Samples	Bandgap range (eV)
Parent	0.40 - 1.91
15 min BMG	1.07 - 2.11
30 min BMG	1.06 – 2.27
45 min BMG	1.02 – 1.97
60 min BMG	1.09 – 2.32
90 min BMG	1.12 – 2.40
120 min BMG	1.15 – 2.25

4.1.2 Graphene thin film preparation and characterization:

Graphene flakes are highly conductive and they have very much non dispersing nature in most of the organic solvent. For that reason we failed to form thin film by Spin Coating method. We have tried by using different rpm with different step but failed. So keeping this point in mind we have tried very simple method to generate thin film which is basically the drop casting method. For drop casting method [32] we used DMF (Dimethylformamide) as solvent and FTO (Fluorine doped Tin Oxide) plate as conducting substrate as we have used these prepared thin films for the purpose of solar cell efficiency calculation. Following method is used to prepare thin films by drop casting method.

Every sample was mixed with DMF solvent as per specification given below:

Sample weight: 10 mg
DMF solvent taken: 1 ml.

Each solution was sonicated for 20 minute using bath sonicator.

Using dropper each sample was dropped (2 – 3 drops) on the cleaned FTO plate.

All the FTO plates were kept very gently in vibration less place for 24 hours.

After 24 hours the whole substrate (FTO) was covered uniformly by the graphene samples. Then these graphene coated FTO plates are characterized by 3D Optical Profiler ZETA INSTRUMENT to view the nature of the produced film and what is the average roughness of the films. Here we have shown below the 3D images of produced films and after that we have plotted the root mean square roughness vs milling time to see the variation of film thickness with milling time.
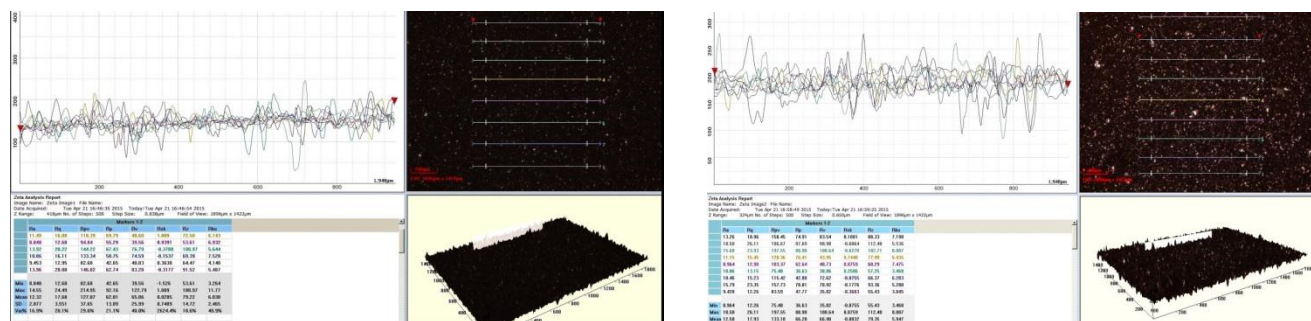
Parent sample

45 min. BMG
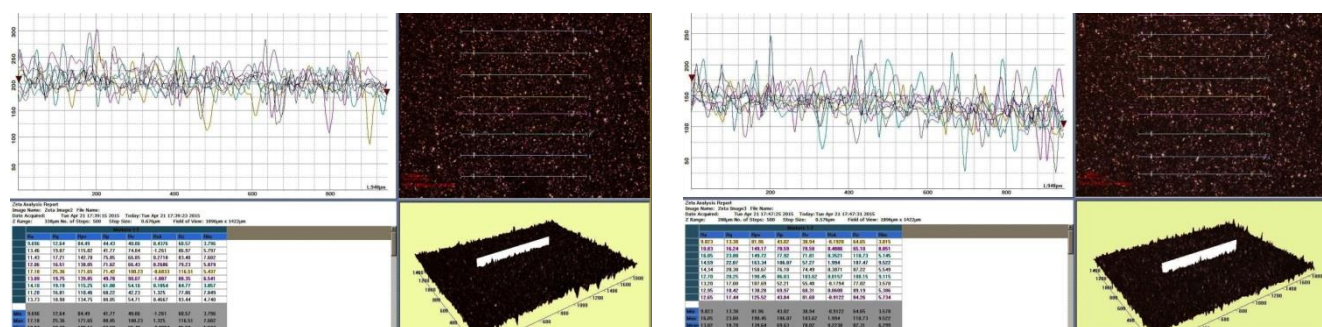
1 hour BMG

1.5 hour BMG

2 hour BMG

Figure 20: *3D OPTICAL ZETA Profiler images of all samples.*

Figure 21: *Variation of root mean square thickness with milling time.*

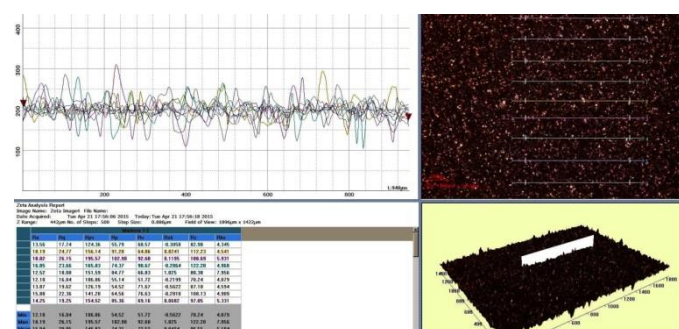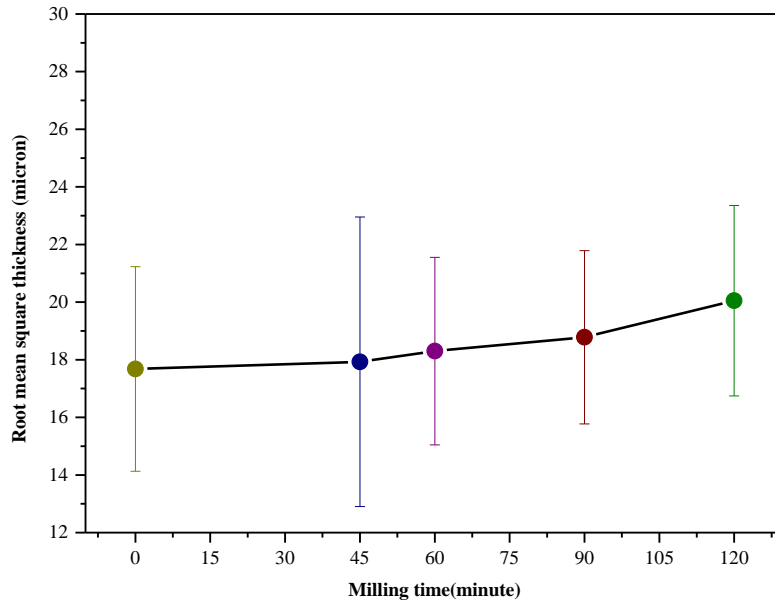From the above graph we conclude that all the films which were produced by drop casting method are more or less same thickness of nearly 15 micron in average and such films are used to measure effiency of solar cells .

4.2 Solar cell Efficiency measurement of samples:

For the every samples we have measured the solar cell efficiency using Photo Emission Tech − Solar Simulator to know how the efficency is changing with produced strain on the graphene sheet. For that measurement we have used 1 sun = 1000 watt/m^2 irradiance as standard light source and callibration voltage of the instrument as 16.7mV DC. Every samples are irradiated and I-V characteristic of the samples are studied to get the efficiency of solar cell. The formula used to measured the efficiency in given below:

$$\eta = \left(\frac{I_{max} * V_{max}}{Area * Irradiance}\right) * 100\%$$

Where, η = Efficiency.

I_{max} = Maximum current in plot.
V_{max} = Maximum voltage.
Irradiance = 1sun(1000watt/m^2)

Now we have plotted the I-V graph for all samples as below:
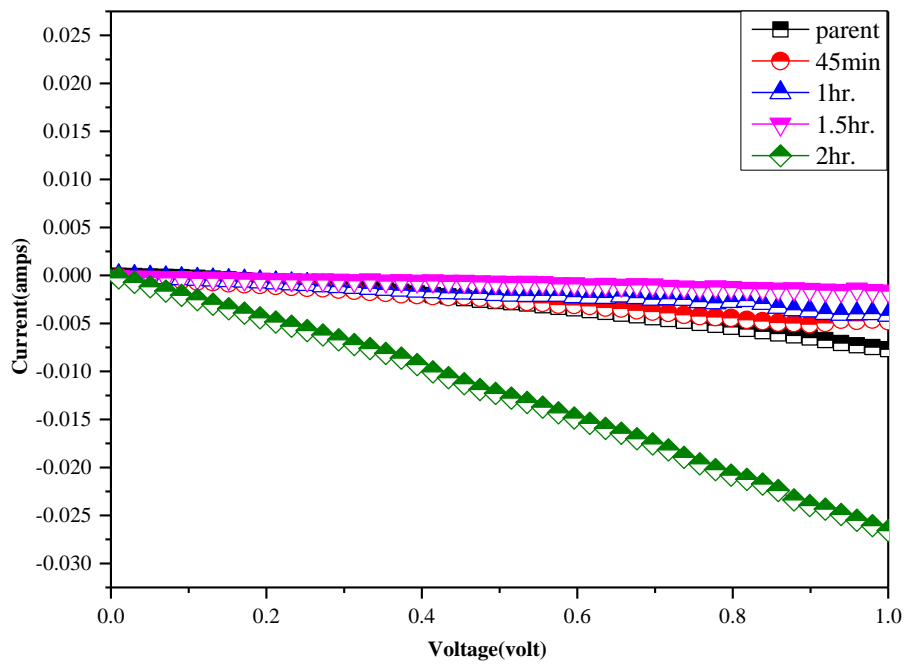
Figure 22: *I-V characteristic of solar cell using different ball milled samples with different time scale. .*

From the above given formula we have calculated efficiency of all the samples and from that we could see an enhancement in the effiency of the solar cell from parent one to 2 hour milled sample. Such details are given below in tabular form:

Sample	Efficiency (%)
Parent	0.00008
45 min. BMG	0.000498
1 hour BMG	0.000545
1.5 hour BMG	0.00136
2 hour BMG	0.00183

Though the efficiency is very less there is a marginal increment in the effiency of the solar cell as a result of compressive strain. From XRD results we could see that there is a peak which corresponds to the graphene oxide. As a result we are unable to say strongly that the band gap opening is compeltely due to graphene. We believe that there is a contribution from the grapene for the bandgap values that we observed in addition to the contribution from the graphene oxide.
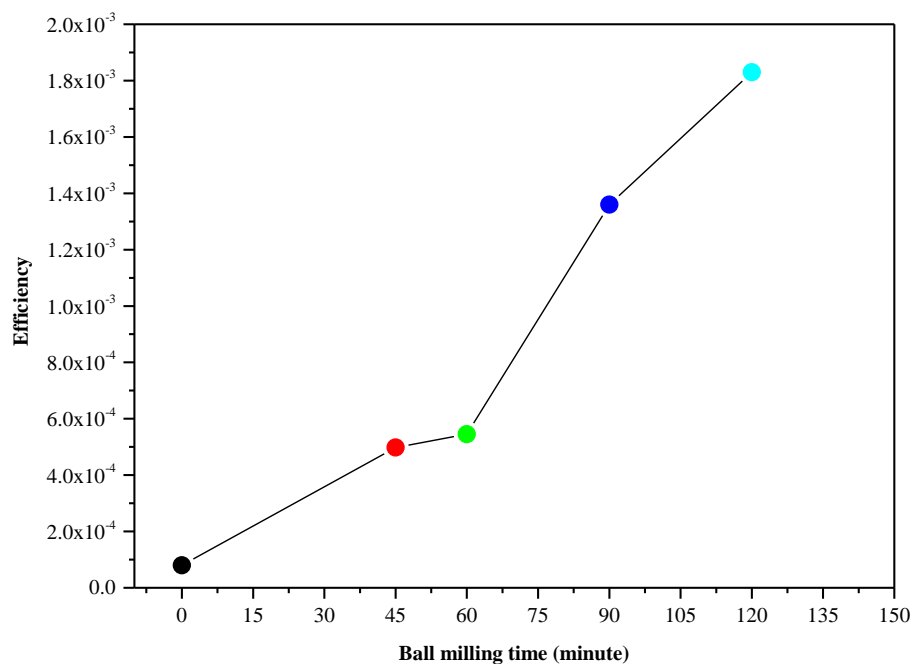
Figure 23: *Increment in efficiency of graphene samples with ball milling time.*

- Chapter 5 -

Results and Discussions

In result and discussion we will concentrate what we have got from our experimental and theoretical studies about the graphene samples and from that what conclusion we can get.

5.1   XRD spectra analysis:

- From X-Ray diffraction data analysis we could see there exists a peak at $2\theta = 26.66^0$ for all samples which is due to graphene nature of the sample. In addition to the peak which corresponds to graphene we also could see a peak pertinent to the graphene oxide at $2\theta = 11.9^0$.

- X-Ray diffraction highest intensity peak doesn't change with respect to ball milling time which essentially indicates that the structure remains same although we have applied compressive strain.

- Average crystallite size is calculated from Scherrer's formula for different milling times. Such calculations indicate that with respect to milling time, average crystallite size decreases. For these calculations we have used the Scherrer's constant as $K = 1.84$.

5.2   Raman spectra analysis:

- From Raman spectral data analysis during our experiment for graphene there are three main peaks namely G peak, 2D peak and D peak. G peaks corresponds doubly degenerate in-plane sp^2 C-C stretching mode and this band represents the planar configuration of the graphene sheet. 2D band represents the two phonon lattice vibrational process and it is called an overtone of the D-band. It does not represent the defect on the graphene sheet. D band represents disorders in the graphene sheets. Sometimes it is called as the disorder band or the defect band. This band originates from the result of a one phonon lattice vibrational process. In our sample D band is very prominent so we can say that there is lot of defect originated on graphene sheet.

- There is a shifting in the G band towards lower wavenumber indicates that the application of compressive strain on graphene upon ball milling time .

- No shift in the D band corresponds to the number of layers in the parent and ball milled compounds are nearly equal. If we curve fit the D band then we can see for every sample only one singe sharp peak is fitted so from that we can confirm that fact [33].

- There is a striking coincidence between the crystallite size which is calculated by Scherrer's formula and one which is calculated using the formula given by Tuinstra and Koenig *et al* [30]. The latter formula is to calculate the crystallite size from Raman spectra whereas the former one is to calculate from XRD. Both the calculations indicate that with respect to ball milling time, the average crystallite size decreases.

5.3 *Theoretically simulated graph analysis:*

- Using GAUSSIAN 09 software we could clearly see that upon compressive strain on graphene, the G peak which corresponds to graphene shifts to lower wave number. In contrast, for the tensile strain, G peak shifts towards higher wave number.

- HOMO LUMO energy analysis indicates that upon increasing disorderness, HOMO LUMO energy difference increases.

5.4 *UV-Vis NIR spectra analysis:*

- From UV-Vis spectral data analysis we came to the conclusion that for graphene there is no sharp absorption peak in the spectra. The peak at 257 nm shows some absorption but the peak is not so sharp to calculate the band gap directly from that.

- So to calculate the bandgap of different ball milled sample we used the Tauc plot and we could conclude from our study that for graphene related samples we cannot calculate bandgap directly so we have to implement the Tauc plot for that.

- Implementing the Tauc plot we could see that there is incremental nature of band gap energy with increase in ball milling time.

- From the value of bandgap measured by the Tauc plot we got the bandgap of parent graphene sample ranging from 0.40 eV to 1.91 eV but we know that for graphene there is no bandgap. Keeping this point in mind if we analyze the XRD data we could see that there is a peak at 2θ = 11.9^0 which corresponds to graphene oxide (GO) peak, so we could say that not only the pure graphene character is there in our samples but also there is presence of graphene oxide which may be responsible for this bandgap in our experimented samples.

5.5 Graphene thin film analysis:

- Using spin coating method we deposited thin films of ball milled graphene. Essentially we have tried various methods like spin coating, dip coating and drop casting method. Among these we could realize that drop casting method is the best method to produce a thin film on FTO substrate. Due to non-soluble nature of graphene in maximum organic solvent it is very tedious to generate thin film on FTO substrate by Spin Coating method.

- Films which were prepared by drop casting method were characterized under 3D Optical ZETA Profiler. After performing analysis we could see that thickness of all the films are essentially same. We also could realize from the above analysis is that drop casting method is effective one to produce graphene thin film.

5.6 Solar Cell efficiency measurement data analysis:

- Efficiency of solar cell is measured using PET solar simulator in the form of I – V characteristics for all the ball milled and drop casted thin films. Although the efficiency is small, we could see that upon ball milling time, efficiency increases.

5.7 Conclusion:

From the powder x – ray diffraction technique, we could confirm that the graphene which is used for the present measurements consists of hexagonal structure and with space group P6$_3$mc. In addition to the intense reflections (002) from graphene, we also could see a peak which is related to graphene oxide (001). Hence, we believe that the properties which we would discuss will be of graphene + graphene oxide. From the Raman spectroscopy, the G peak which corresponds to breathing of sp^2 bond shifts to lower wave number which is due to compressive strain. D peak which corresponds to defects in graphene remains constant with respect to wave number. However, the intensity increases

as a result of increase in defects. I_D/I_G ratio increases, which essentially means that the defect increases with respect to ball milling time. 2D peak which corresponds to double phonon scattering remains constant and there is no shift for the above. Calculated band gap values from absorption spectra are in the range of 0.4 – 2.25 eV. If we think logically, as graphene is zero band gap semiconductor or semi metal, it should not give any band gap value. However, from the measurements that we performed we could see a gap opening of 0.4 eV in the parent form. What we believe is that the gap opening of 0.4 eV may have contribution from graphene oxide, which we could realize from x – ray diffraction measurements. Using these ball milled graphene we could prepare thin films on FTO substrate using drop casting method. Such films were used to measure the efficiency of solar cells. We also could see the surface morphology of films using 3D ZETA profiler and looks like the surface is smooth everywhere with the thickness of 18μm. As the ball milling time increases, the efficiency of solar cell increases from 8×10^{-5} – 1.8×10^{-3}, which is the indication that band gap of graphene is varying with respect to milling time. We also have performed theoretical calculations using Gaussian 09 software, which is to calculate the available Raman modes with respect to change in the bond angles or bond lengths. As bond length between two sp_2 hybridized carbon changes, the G peak of graphene shifts to lower wave number, which is in accordance with our experimental results. However, the values of wave number don't match with respect to experimental one which could be due to the kind of structure that we have used in our simulations.

5.8 Outlook:

In this thesis work we have proposed a new method to create bandgap in graphene which was prepared by CVD technique. Already many research groups are trying to create bandgap in graphene so that it can be more promising material in optoelectronic applications. Our present work suggests a very cheap and effective method to produce bandgap in graphene. In addition, we have measured the solar cell efficiency of all ball milled samples and from there also we got a sequential increment in the efficiency.

Now due to some constraint in availability of CVD equipment we have done all the experiment and characterization using commercially available graphene from Redex Tech. Pvt. Limited. So we are unable to do experiment with pure graphene sample as a result of the fact that the present sample consists of small percentage of graphene oxide. But currently in our laboratory we are planning to produce graphene with CVD technique which may be useful for our future studies.

References

[1] K. S. Novoselov, A. K. Geim, S. V. Morozov, D. Jiang, Y. Zhang, S. V. Dubonos, I. V. Grigorieva, and A. A. Firsov, Science **306** (5696), 666 (2004).

[2] A. K. Geim and K. S. Novoselov, Nature materials **6** (3), 183 (2007).

[3] Martin A. Green, Progress in Photovoltaics: Research and Applications **17** (3), 183 (2009); Martin A. Green, Keith Emery, Yoshihiro Hishikawa, and Wilhelm Warta, Progress in Photovoltaics: Research and Applications **17** (5), 320 (2009).

[4] Alexander A. Balandin, Nat Nano **8** (8), 549 (2013).

[5] H. Vita, S. Bottcher, K. Horn, E. N. Voloshina, R. E. Ovcharenko, T. Kampen, A. Thissen, and Y. S. Dedkov, Scientific reports **4**, 5704 (2014).

[6] X. Miao, S. Tongay, M. K. Petterson, K. Berke, A. G. Rinzler, B. R. Appleton, and A. F. Hebard, Nano letters **12** (6), 2745 (2012).

[7] Richard Balog, Bjarke Jorgensen, Louis Nilsson, Mie Andersen, Emile Rienks, Marco Bianchi, Mattia Fanetti, Erik Laegsgaard, Alessandro Baraldi, Silvano Lizzit, Zeljko Sljivancanin, Flemming Besenbacher, Bjork Hammer, Thomas G. Pedersen, Philip Hofmann, and Liv Hornekaer, Nature materials **9** (4), 315 (2010).

[8] Marc Dvorak, William Oswald, and Zhigang Wu, Sci. Rep. **3** (2013).

[9] L. M. Malard, M. A. Pimenta, G. Dresselhaus, and M. S. Dresselhaus, Physics Reports **473** (5-6), 51 (2009).

[10] Frank Schwierz, Nat Nano **5** (7), 487 (2010).

[11] L. M. Malard, M. A. Pimenta, G. Dresselhaus, and M. S. Dresselhaus, Physics Reports **473** (5–6), 51 (2009).

[12] Michael J. Frisch, G. W. Trucks, H. Bernhard Schlegel, Gustavo E. Scuseria, Michael A. Robb, James R. Cheeseman, Giovanni Scalmani, Vincenzo Barone, Benedetta Mennucci, G. A. Petersson, H. Nakatsuji, M. Caricato, Xiaosong Li, H. P. Hratchian, Artur F. Izmaylov, Julien Bloino, G. Zheng, J. L. Sonnenberg, M. Hada, M. Ehara, K. Toyota, R. Fukuda, J. Hasegawa, M. Ishida, T. Nakajima, Y. Honda, O. Kitao, H. Nakai, T. Vreven, J. A. Montgomery Jr., J. E. Peralta, François Ogliaro, Michael J. Bearpark, Jochen Heyd, E. N. Brothers, K. N. Kudin, V. N. Staroverov, Rika Kobayashi, J. Normand, Krishnan Raghavachari, Alistair P. Rendell, J. C. Burant, S. S. Iyengar, Jacopo Tomasi, M. Cossi, N. Rega, N. J. Millam, M. Klene, J. E. Knox, J. B. Cross, V. Bakken, C. Adamo, J. Jaramillo, R. Gomperts, R. E. Stratmann, O. Yazyev, A. J. Austin, R. Cammi, C. Pomelli, J. W. Ochterski, R. L. Martin, K. Morokuma, V. G. Zakrzewski, G. A. Voth, P. Salvador, J. J. Dannenberg, S. Dapprich, A. D. Daniels, Ödön Farkas, J. B. Foresman, J. V. Ortiz, J. Cioslowski, and Douglas J. Fox, Gaussian 09 (Gaussian, Inc., Wallingford, CT, USA, 2009).

[13] Axel D. Becke, The Journal of Chemical Physics **98** (7), 5648 (1993).

14   P. Jeffrey Hay and Willard R. Wadt, The Journal of Chemical Physics **82** (1), 270 (1985).

15   I. W. Frank, D. M. Tanenbaum, A. M. van der Zande, and P. L. McEuen, Journal of Vacuum Science & Technology B **25** (6), 2558 (2007); C. Y. Wang, K. Mylvaganam, and L. C. Zhang, Physical Review B **80** (15), 155445 (2009).

16   Changgu Lee, Xiaoding Wei, Jeffrey W. Kysar, and James Hone, Science **321** (5887), 385 (2008).

17   Yuanbo Zhang, Yan-Wen Tan, Horst L. Stormer, and Philip Kim, Nature **438** (7065), 201 (2005).

18   J Hass, W A de Heer, and E H Conrad, Journal of Physics: Condensed Matter **20** (32), 323202 (2008).

19   Qingkai Yu, Jie Lian, Sujitra Siriponglert, Hao Li, Yong P. Chen, and Shin-Shem Pei, Applied Physics Letters **93** (11), 113103 (2008).

20   X. Li, W. Cai, J. An, S. Kim, J. Nah, D. Yang, R. Piner, A. Velamakanni, I. Jung, E. Tutuc, S. K. Banerjee, L. Colombo, and R. S. Ruoff, Science **324** (5932), 1312 (2009).

21   Ning Zhan, Mario Olmedo, Guoping Wang, and Jianlin Liu, Carbon **49** (6), 2046 (2011).

22   Dmitry V. Kosynkin, Amanda L. Higginbotham, Alexander Sinitskii, Jay R. Lomeda, Ayrat Dimiev, B. Katherine Price, and James M. Tour, Nature **458** (7240), 872 (2009).

23   Mohammad Choucair, Pall Thordarson, and John A. Stride, Nat Nano **4** (1), 30 (2009).

24   Ahmad Monshi, Mohammad Reza Foroughi, and Mohammad Reza Monshi, World Journal of Nano Science and Engineering **02** (03), 154 (2012).

25   O. A. Maslova, M. R. Ammar, G. Guimbretière, J. N. Rouzaud, and P. Simon, Physical Review B **86** (13) (2012).

26   R. Beams, L. Gustavo Cancado, and L. Novotny, Journal of physics. Condensed matter : an Institute of Physics journal **27** (8), 083002 (2015).

27   M. Huang, H. Yan, C. Chen, D. Song, T. F. Heinz, and J. Hone, Proceedings of the National Academy of Sciences of the United States of America **106** (18), 7304 (2009).

28   Otakar Frank, Georgia Tsoukleri, John Parthenios, Konstantinos Papagelis, Ibtsam Riaz, Rashid Jalil, Kostya S. Novoselov, and Costas Galiotis, ACS Nano **4** (6), 3131 (2010).

29   Noel M. O'Boyle, Adam L. Tenderholt, and Karol M. Langner, Journal of computational chemistry **29** (5), 839 (2008).

30   F. Tuinstra and J. L. Koenig, The Journal of Chemical Physics **53** (3), 1126 (1970).

31   Hsin-Cheng Hsu, Indrajit Shown, Hsieh-Yu Wei, Yu-Chung Chang, He-Yun Du, Yan-Gu Lin, Chi-Ang Tseng, Chen-Hao Wang, Li-Chyong Chen, Yu-Chuan Lin, and Kuei-Hsien Chen, Nanoscale **5** (1), 262 (2013).

32   A. A. M. Farag and I. S. Yahia, Optics Communications **283** (21), 4310 (2010).

33   A. C. Ferrari, J. C. Meyer, V. Scardaci, C. Casiraghi, M. Lazzeri, F. Mauri, S. Piscanec, D. Jiang, K. S. Novoselov, S. Roth, and A. K. Geim, Physical Review Letters **97** (18) (2006).